Large-scale and synoptic meteorology in the south-east Pacific during the observations campaign VOCALS-REx in Spring 2008

Thomas Toniazzo*

Steve J. Abel

Robert Wood

Carlos R. Mechoso

Grant Allen

Leonard C. Shaffrey

Abstract

We present a descriptive overview of the meteorology in the south eastern subtropical Pacific during the VOCALS-REx intensive observations campaign, which took place in October and November 2008. We provide a summary of the day-to-day meteorological and cloud conditions. Our main aim is to provide some broader spatial and temporal meteorological context for the measurements made during VOCALS-REx, attempting to link the large-scale conditions of the atmospheric circulation with the locally observed conditions, also with a view of estimating the representativity of the specific season that was sampled by VOCALS-REx.

1 Introduction

The marine stratocumulus (Sc) systems of the subtropical anticyclones cause a large negative radiative forcing for the global climate system. They are also associated with oceanic upwelling systems of enormous

*NCAS-Climate, Department of Meteorology, University of Reading, RG6 6BB, UK; t.toniazzo@reading.ac.uk

biological productivity. Such association make them into fundamentally important building blocks of the present-day climate system.

Unfortunately, they are also some of the areas less well-understood or well-modelled in climate science. Uncertainties in top-of-the-atmosphere short-wave forcing from the tropical Sc decks seriously affect the projected climate sensitivity under greenhouse-gas forcing (Bony and Dufresne, 2005). Moreover, climate simulations of present-day (and, by implication, historical) conditions consistently show both large errors in the climatology of these regions (de Szoeke and Xie, 2008), and a very high sensitivity to it, affecting the global tropical circulation via a series of coupled ocean-atmosphere feedbacks (Ma et al., 1996), which affect both the mean climate and its modes of variability (Toniazzo, 2009). The modelled Sc in turn are sensitive to feedbacks between radiation and turbulence in the maritime boundary-layer (MBL) that tend to exacerbate errors (Konor et al. 2009).

In part to address some of these issues, a concentrated observational and modelling study has been underway that focusses on the south-eastern Pacific (SEP) off the western coast of South America, where the most persistent tropical Sc decks are found (Klein and Hartmann, 1993). The international research project, called VOCALS (VAMOS ocean-cloud-atmosphere-land study), included an intensive observations campaign in the SEP (VOCALS-REx), between 1 October and 2 December, 2008. An introduction to VOCALS, and a detailed overview of VOCALS-REx operations and observations, is provided in Wood et al. (2010).

Our primary goal in this contribution, is to provide a meteorological context for VOCALS-REx observations. In doing so, we aim to highlight the role of synoptic and large-scale atmospheric forcing in controlling changes to the Sc deck. This addresses one of the core science questions of VOCALS, namely to what extent cloud microphysical processes, including aerosol interaction, affect the cloud cover in tropical Sc areas. Several inroads have been made already. Garreaud et al. (2002) have shown that sub-synoptic systems that arise from the interaction between synoptic forcing and the Andean orography significantly affect Sc cover over time-scales of a few days. From their analysis of satellite and sea-level pressure data, George and Wood (2010) have argued that, more generally, sub-seasonal variability in cloud properties is to a significant extent controlled by meteorological conditions. In the context of VOCALS-REx, Rahn and Garreaud (2010b) have shown that the observed variability in MBL depth, and in part of the associated cloud cover, was largely

dependent on synoptic forcing in the SEP area. Additional evidence of meteorological controls is given in Zuidema et al. (2009) and Painemal et al. (2010).

With the help of data from the UK Met Office operational forecasts of the relevant period (Abel et al. 2010), here we attempt to synthesise and complement this information and provide a tentative interpretation for the link between Sc cloud cover and the circulation in the SEP.

2 Data sources

We base most of the following discussion on data from the analysis fields and 21-hour forecasts (at 3-hourly intervals) of the UK Met Office global operational forecast model. Abel et al. (2010) provide a validation for the limited-area version of this model in the SEP for the period of interest. They show that, in general, the model fields are consistent with in-situ observations when maritime areas well away from the coast are considered. In such areas, the differences between the limited-area model and the lower-resolution global operational forecast model (40km compared to 15km) are very small in all quantities that are discussed in this paper. Accordingly, we mostly focus our analysis on the maritime areas of the SEP. The advantage of the global forecast model is both its spatial coverage and its longer temporal coverage of the VOCALS-REx period. Here we consider data for the whole of October and November 2008. The longer-term climatological context and back-trajectories are obtained from the ECMWF operational analyses and from the ERA-Interim reanalysis (Simmons et al., 2006). We also refer to datasets obtained from the observational activities of the VOCALS-REx campaign. These include ship-based radiosonde profiles, and measurements of SSTs, surface air temperatures and winds (see Wood et al., 2010; cf. also Zuidema et al., 2009; Bretherton et al., 2010). In addition, we use visible and infra-red imagery from the NOAA geostationary meteorological satellite GOES-10, the satellite-derived SST products OSTIA (Stark et al. 2007), and the Optimal Interpolation dataset from NOAA (Reynolds et al., 2002).

3 The average atmospheric circulation in the SEP

From a large-scale perspective, the SEP is part of the source region of the surface trade-winds of the southern tropical Pacific (e.g. Hastenrath 1991), under the descending, radiatively cooling branch of the

Walker-Hadley circulation in the Pacific. The large-scale subsidence over the SEP is connected with the semi-permanent areas of cumulus convection and large-scale ascent over the West Pacific and the Maritime Continent (the archipelago comprising Java, Sumatra, Borneo and New Guinea). Seasonally, it is also dynamically linked with the inter-tropical convergence zone (ITCZ) north of the Equator, associated with the western warm pool extending from the Atlantic Caribbean to the Gulf of Panama, with the south-American Monsoon over the Amazon and the eastern Andean slopes, and with the south-Pacific convergence zone (SPCZ) in the southern west Pacific.

Near the surface, the SEP is located at the eastern end of the south-Pacific sub-tropical anticyclone, characterised by steady, divergent winds, which intensify near land into a low-level jet parallel to the coast. A permanent inversion with extensive strato-cumulus cloud (Sc) separates the cool, moist marine boundary layer (MBL) from the warm and dry free troposphere (FT, Figure 1). The cool MBL temperatures in the SEP result from a combination of atmospheric and oceanic processes. While orographic blocking increases the static stability and contributes in maintaining the strong inversion capping the MBL (Richter and Mechoso, 2006; Wyant et al. 2010), cool MBL temperatures are consistent with the low moist static energy of the very dry free-tropospheric air above (Takahashi and Battisti, 2007). Within the MBL, the flow of cool, dry air over the sea-water generates evaporation, and the Sc cover, stabilised by the inversion, limits the short-wave (SW) radiation absorbed by the ocean by an amount of the order of one hundred W/m^2 (e.g. Colbo and Weller, 2007). The positive residual net heat flux into the ocean (Colbo and Weller, 2007) is offset by cold oceanic advection, aided by the wind-forced coastal upwelling. The relative role of each of these processes to maintain the observed thermal and dynamical state of the MBL in the SEP has long been the subject of active investigation (e.g. Ma et al., 1996; Zheng et al., 2010).

The surface flow is dynamically coupled at upper levels in the troposphere with the subtropical jet stream. Conditions in the SEP are influenced by the transport of momentum and tracers in and across the jet stream, and, recurrently, directly affected by baroclinic activity in the southern mid-latitudes. Particularly noticeable is the occurrence of coastally-intensified cyclones, or coastal lows, which initially develop upstream of the SEP and are affected by the Andean orography. In particular, trailing cold fronts are observed as far north as 20S between autumn and spring (Seleuchi et al., 2006; Barret et al., 2009; Rahn and Garreaud, 2010; a further example, for October 23-24, can be seen in Figure 9).

The level of the MBL-top inversion represents the scale-height of the cold surface anticyclone, which disappears above 700hPa (Figure 1). East of the surface anticyclone, the mean wind veers dramatically, with a mean westerly flow aloft replacing the southerly flow in the MBL. At the northern edge of the anticyclone, near 20S where VOCALS-REx took place, the mean MBL winds also have a significant easterly component, while above the inversion in the FT there is a weak mean northerly component. Directional variability is extremely small in the MBL, but it is generally much more pronounced on synoptic time-scales in the FT.

The relationship between the mean atmospheric flow and the thickness of the cool MBL is illustrated in Figure 1, which shows isobars and isoentropes at various heights, together with the line where the inversion crosses the relevant altitude (thick, pink contour-line in the sections at 1620m and 2420m). Here and throughout this paper, we diagnose the height of the inversion as the location of maximum vertical gradient in potential temperature. For the model fields, this is estimated by first differences, and the inversion height at any given point in time and space corresponds to one of the model helf-levels. To first order, the thermal wind in the lower troposphere reflects thickness variations of the cool MBL, rather than horizontal gradients in the MBL temperature itself.

Above the inversion in the free troposphere (Figure 2), prominent regional features are associated with the heat sources over the elevated topography of the Andes, especially the Peruvian Andes and the Bolivian altiplano, and over areas of moist convection in the Atlantic Warm Pool and the Amazon basin. A Gill-type (Gill 1980) double anticyclonic pattern is visible in Figure 2(b). Its southern branch appears reinforced by the shallower heating over the Andes (Figure 2(a)) and results in an anticyclonic turning of the upper-tropospheric winds above the SEP near the continent. As the spring season progresses, insolation and convective activity gradually increase and move southwards, resulting in a strengthening and a southward extension of the pattern shown in Figure 2(b). As well as on the mean circulation, in section 8 we argue that this also affects the character of the diurnal cycle over the SEP.

The thermally direct, mean cell associated with the Andes is most evident in the meridional transects shown in Figure 3, especially near the coast. Further offshore, the structure of the circulation partly results from the average of a diurnal gravity wave (Garreaud and Munoz 2004, Wood et al., 2009; see also section 8 below), characterised by an outward-propagating (in the SSW direction) line of positive vertical velocity in

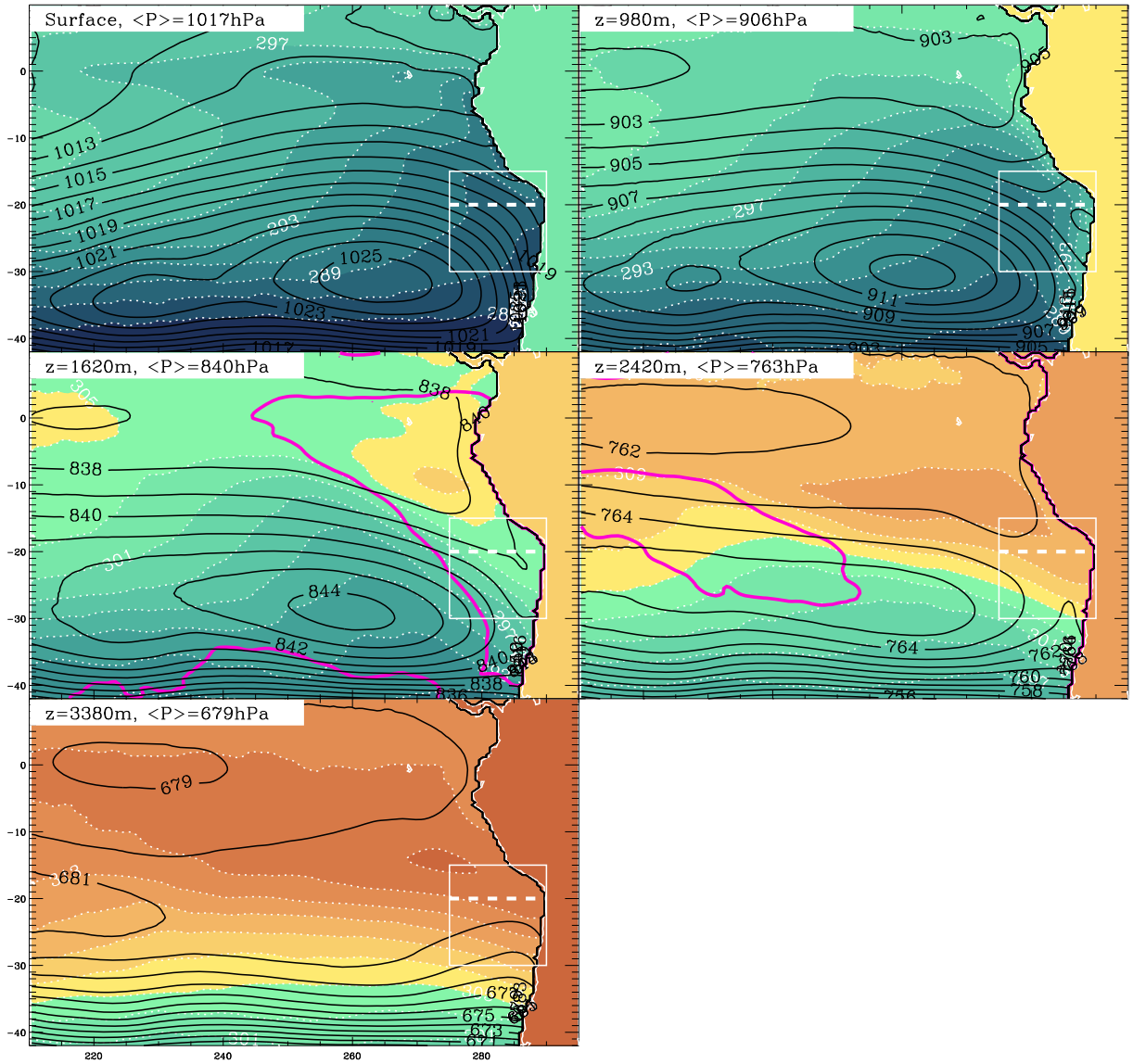

Figure 1: Potential temperature (colour-coded, dotted contours, in K) and pressure (full black lines, in hPa) for the October-November 2008 mean in the south-east Pacific, at the surface and four different altitudes, as indicated. The pink contour lines in the third and fourth panels indicates where the diagnosed inversion intersects the horizontal section. The white box with the thick dashed line along 20S marks the area where VOCALS-REx operations took place. Data from the UKMO global operational analysis.

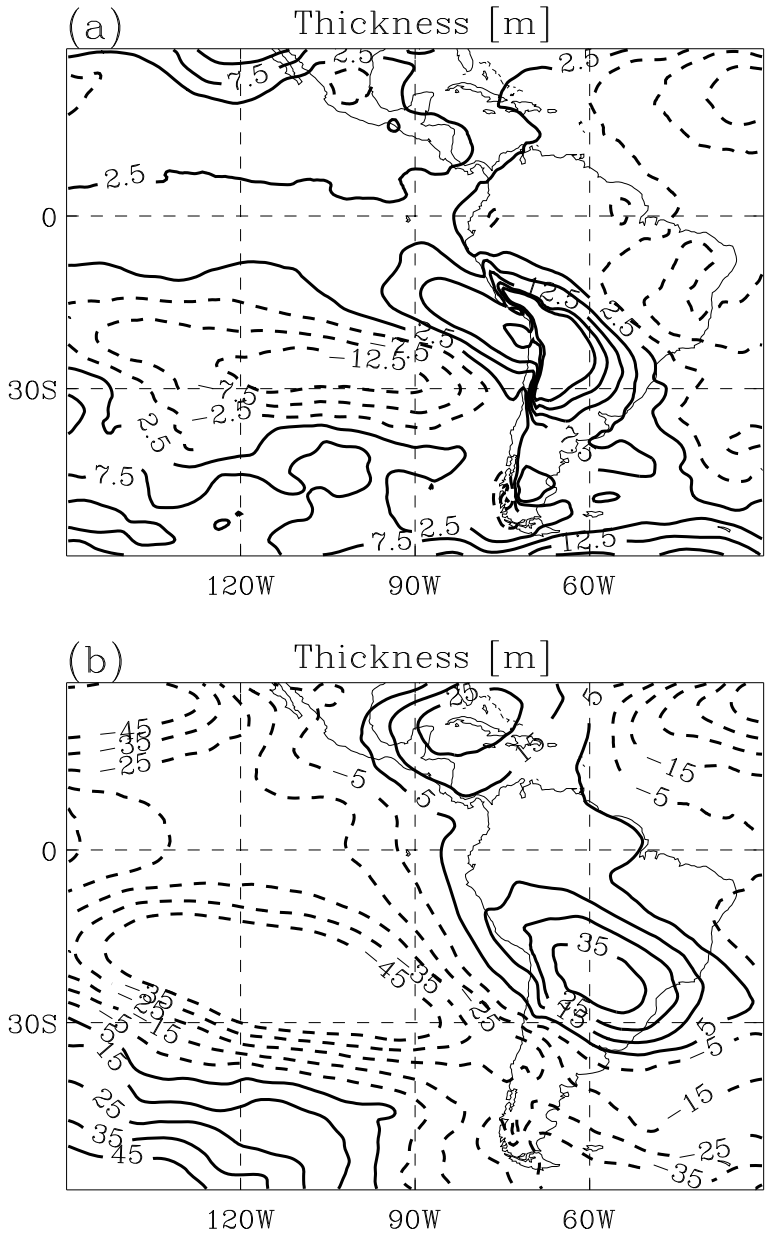

Figure 2: Zonally asymmetric components of the 500hPa-700hPa and 200hPa-500hPa geopotential thickness fields (panels (a) and (b), respectively) in the eastern-Pacific/south-American sector. Shown are the time-means for the period between 1 October 2008 and 30 November 2008. Positive values are shown by the solid contours, negative values by broken contours. In panel (a), the contour interval is 5m; in panel (b), it is 10m. . Data from UKMO operational analysis.

the lower troposphere. Over the lower terrain to the North of the orography, inside the Amazon basin, there is the mean ascent with a deeper structure than that directly above the orography, consistently with moist convection. Mean southward advection, and subsequent descent, of the air-masses lofted in this convective activity can carry them into the VOCALS-REx area around 20S (see later discussion in section 4.2).

In the upper troposphere, the zonal flow (colour-coded in Figure 3) is dominated by the subtropical jet-stream, which is associated with sloping isoentropes (shown as white lines), and extends as far North as 20S. The flow in the meridional plane is generally indicative of radiative cooling, compensated by subsidence. Further south there is ascent associated with mid-latitude baroclinic activity. In the MBL, an easterly thermal jet is located near the Peruvian coast. Moving west, the easterly acceleration of the flow is associated with a line of meridional convergence above inversion at 22S. This is diurnally modulated in a transient flow resembling that of an internal gravity wave (Section 8).

Figure 4 shows zonal transects of the mean circulation in the VOCALS-REx area. Considering first the section along 29S, the flow is characterised by mean westerlies aloft and easterlies in the MBL. The mean vertical wind is downward everywhere except in the lower free troposphere near the orography, where a distinct barrier flow is noticeable, with poleward wind allowing for vortex stretching. Consistently with the high stability in the free troposphere, the flow across the Andes is subcritical in terms of its Froude number. It Rossby number, however, is, on average, close to one, with a characteristic pressure maximum above and upstream of the crest, balanced by the southerly wind component which extends the barrier flow along the western flanks aloft and eastwards. The increases pressure upstream of the orography associated with the zonal flow affects the pressure distribution at the surface (Richter and Mechoso 2006) and contributes to the surface divergence in the VOCALS-REx area.

Associated with the south-American land-mass, there is a mean temperature front across the mountain chain, with a positive zonal temperature gradient giving an additional northerly thermal wind component. In the lower reaches of both eastern and western flanks of the orographic ridge, mean updraught occurs, most likely of diabatic origin. However, the updraught is stronger and extends higher on the eastern flank of the Andes, where is is associated with a low-level southerly flow. On the western slopes, consistently with the prevailing dry conditions, the warmer air temperatures in proximity of the terrain are associated with adiabatic descent along the flank of the orography. The downslope flow is suggested in Figure 4, but as it

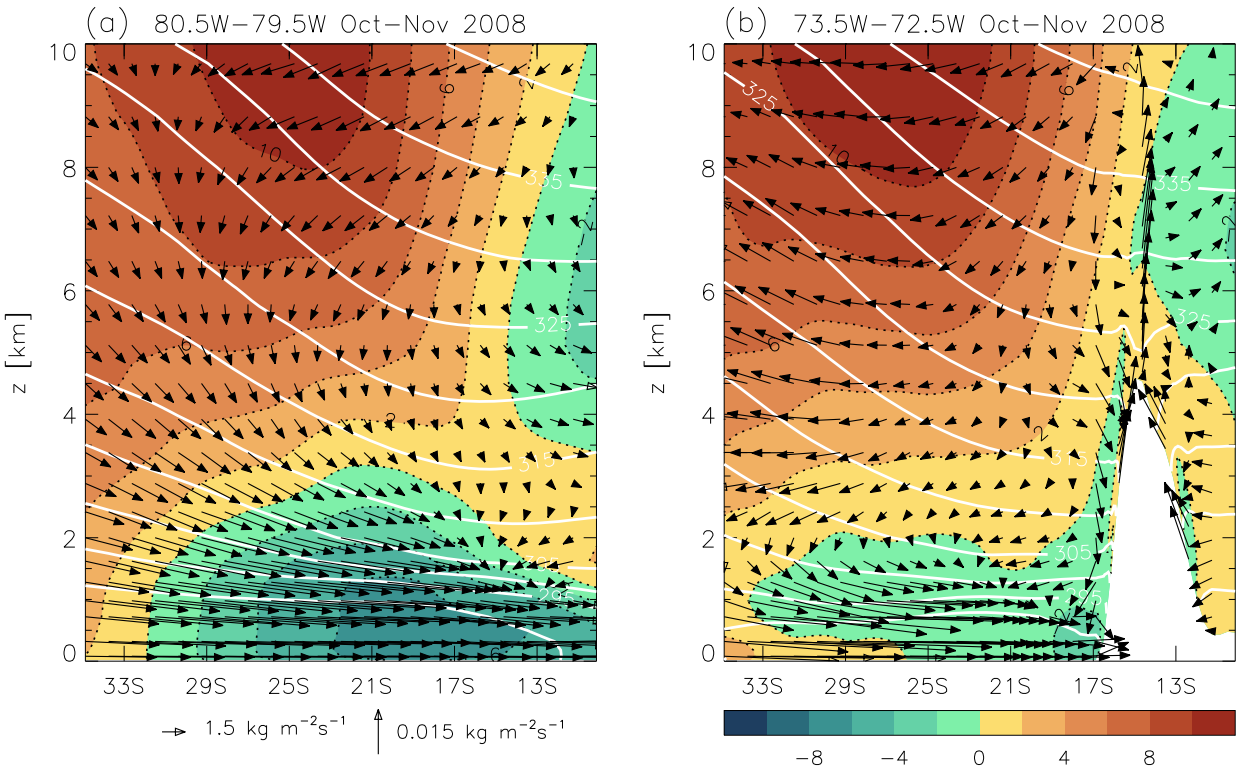

Figure 3: Meridional transects of mean winds and isoentropes during October-November 2008. Winds are multiplied by density to give mass fluxes. Colour-coding shows zonal wind-speed, with contour interval of 2 kg m^{-2} s^{-2}; white lines are contours for the dry potential temperature, with a spacing of 5K. Vector scales for the meridional and the vertical winds are given on the bottom-right. Left: section along 80W. Right: section along 73W. Means from 3-hourly UKMO operational analysis and 3h-21h forecasts are used.

is intrinsically associated with the diurnal circulation of a land-sea and mountain breeze system, it is not accurately represented in the mean winds shown, which suggest warm vertical advection.

In the MBL the most prominent feature of the circulation is the southerly coastal jet (Munoz and Garreaud, 2005). The southerly flow in the MBL is consistent with Sverdrup balance below the level of maximum subsidence (around 500 hPa), associated with radiative cooling, and is maintained by the positive zonal temperature gradient associated with the coastal land-mass.

Along 20S, where most VOCALS-REx observations where taken, the mean flow is similar, but with a

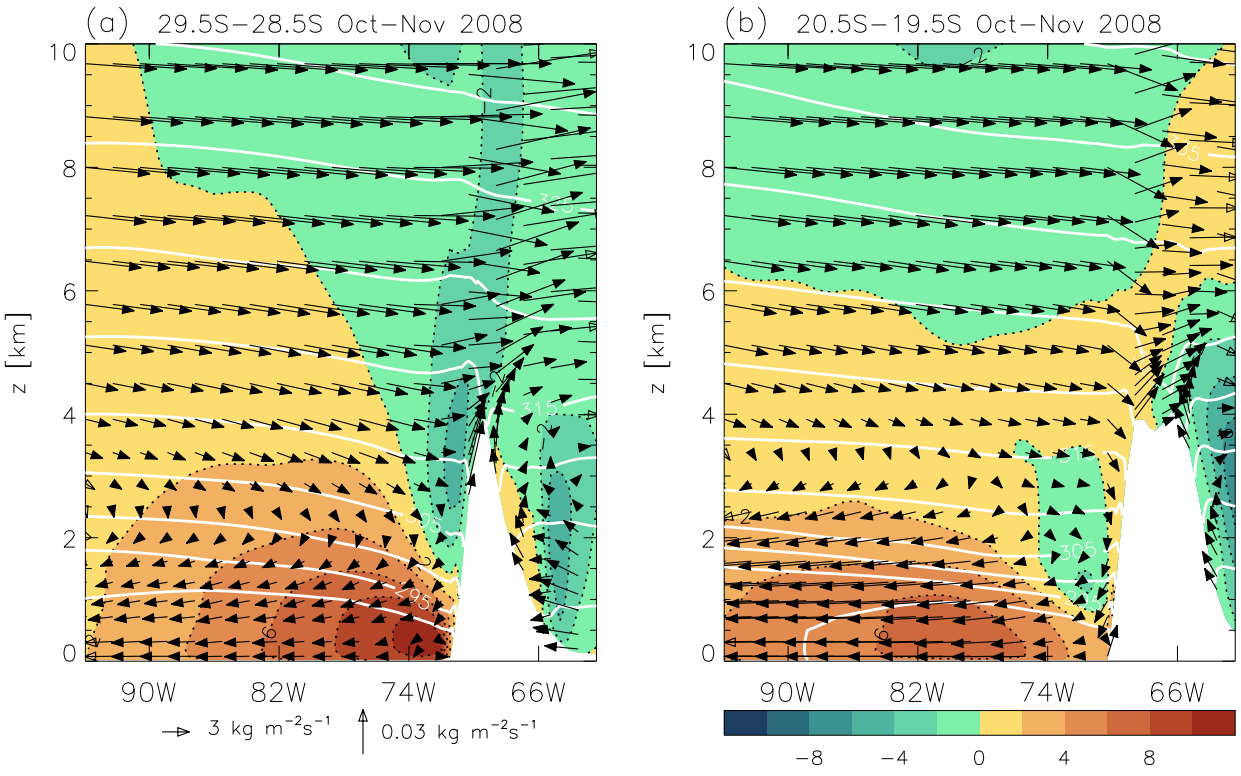

Figure 4: As in Figure 3, but for zonal transects along 29S (left) and 20S (right). Vectors for the vertical and zonal component (scales on the bottom-right), colour-coding for the meridional component. Contour intervals are the same as in Figure 3.

few differences, and complications. Located at the northern edge of the anticyclone and of the subtropical jet, the zonal flow is stronger and more divergent in the MBL, and weaker aloft. The meridional component of the flow is less pronounced, with the maximum wind well away from the coast and no persistent coastal jet.

The flow across the orography has smaller Rossby numbers (partly also due to the wider orographic ridge), and is associated with a weak mean southerly component, suggesting planetary-vorticity balance. Below the level of the ridge, however, the flow appears blocked, and west of the coast there still is a northerly barrier flow. Close to land the mean flow appears to turn southerly, in association with a strong mean upslope wind, suggesting a mean, buoyant surface density current, which converges over the high plateau of the Bolivian Altiplano. Over the upslope surface current, however, there is strong mean descent, possibly

maintaining mass continuity with the zonal flow deceleration aloft. The diabatic forcing associated with the diurnal cycle is likely to be important for the observed mean thermal structure and mean flow. In addition, variability on synoptic time-scales is associated not only with variations in the zonal wind speed, but also with changes, sometimes even in sign, of the meridional and vertical wind components, as the dynamical character of the flow across the orography changes. In general, strengthened zonal flow is associated with enhanced orographic drag and increasing upward and poleward motion over the coastal ocean.

Aloft, the isoentropes have a nearly constant slope and the winds turn northerly everywhere. With a warmer free troposphere and similar MBL temperatures, the inversion is much stronger at 20S than at 30S, and the cloud cover more persistent. Additional features of the flow near 20S arise due to the proximity of the Peruvian orography, which is oriented at an angle along the WNW-ESE direction and intercepts the mean southerly flow in the MBL and the lower FT. As mentioned earlier, the circulation near this ridge has a vigorous diurnal cycle, with larger diurnal variations than those associated with the N-S Andean crest.

4 Characterisation of the meteorology during VOCALS-REx

4.1 General

The VOCALS-REx campaign, which took place in the period between 1 October and 2 December, sampled the eastern flank of the southeastern Pacific subtropical high pressure system.

At the deepest point of the wide bay formed by the southern Peruvian and northern Chilean coastlines, the town of Arica (18°S, 70°W) served as the main operational base of VOCALS-REx. Observations gathering concentrated in the vicinity of 20S, between 72W, near the Chilean coast, and a western-most point at 85W where a WHOI data buoy is located. Along, and within a range of 200-300 km of the coast, ground-, aircraft- and ship-based activities sampled atmospheric data between 30S and 13S. Wood et al. (2010) goiva a comprehensive description of VOCALS-REx operations.

As is typical for austral spring, sea surface temperatures (SSTs) along the coast were cold offshore of the strongest upwelling zones, located both to the south and to the north of the Arica bight, where SSTs had a local maximum (Fig. 5b). Away from the coast, the SST gradient is to the west and northwest.

Within the VOCALS region, surface winds were typically south-southeasterly, from 177^o at 20S,71W to

125^o at 20S,85W. (Fig. 5a). West of 75W, directionality was very steady, with a standard deviation of less than 10^o; this figure raises to about 30^o close to the coast.

The general alignment of the surface winds with the SST gradient implies cold advection in the MBL. This is capped by a strong inversion located at a pressure ranging from 900 hPa near the coast, to about 800 hPa on the open sea in the time average. Away from the coast, significant temporal variations of the inversion height occur, mainly on synoptic time-scales, with heights ranging between 900 hPa and 700 hPa at 90W, and between 930 hPa and 850 hPa at 75W. The temperature jump across this inversion is typically about 15^oC, RH is dramatically reduced from saturation or near -saturation to less than 10%, A thermal wind is associated with the mean gradient in inversion height. Near 20S, the latter is largely aligned with the wind itself, resulting in little directional change (a slight backing), and the wind remains eastward near the coast and north-eastward offshore. An additional thermal wind component above this level is associated with the predominantly meridional mean temperature gradient in the free troposphere. The mean direction changes to between westerly and southerly at 700hPa, with a strong reduction in mean wind-speed. However, wind directional variability also becomes markedly larger (45^o-60^o in standard deviation), increasingly so away from the coast.

The cool, moist, inversion-capped MBL provides the conditions for the maintenance of the extensive stratocumulus cloud. The mean cloud cover from water clouds is shown in Figure 5c, as obtained from MODIS Terra satellite at 10:30 LT. It reaches its maximum within a belt at a distance of 500 km from, and roughly parallel to, the Peruvian coast, with mean values exceeding 90 This region is situated a few hundred km downwind of the maximum in lower tropospheric stability (LTS, Fig. 5d), which is defined the difference between the potential temperature at 700 hPa and the surface. Over most of the region sampled in VOCALS-REx the mean warm-cloud cover exceeded 70 where coastal irregularities and the advection of drier air masses are conducive to local clearings.

Figure 5e,f also show the mean liquid water path (LWP), as determined for cloudy pixels using the visible/near-IR retrievals from MODIS (panel (e)) and from the passive microwave Advanced Microwave Scanning Radiometer (AMSR; panel (f)). The two estimates agree very well within about 500 km of the coast, where the potential contamination of the AMSR estimate by drizzle is limited (as evidenced from VOCALS-REx aircraft observations, Bretherton et al. 2010). Within this region, typical cloud LWP values

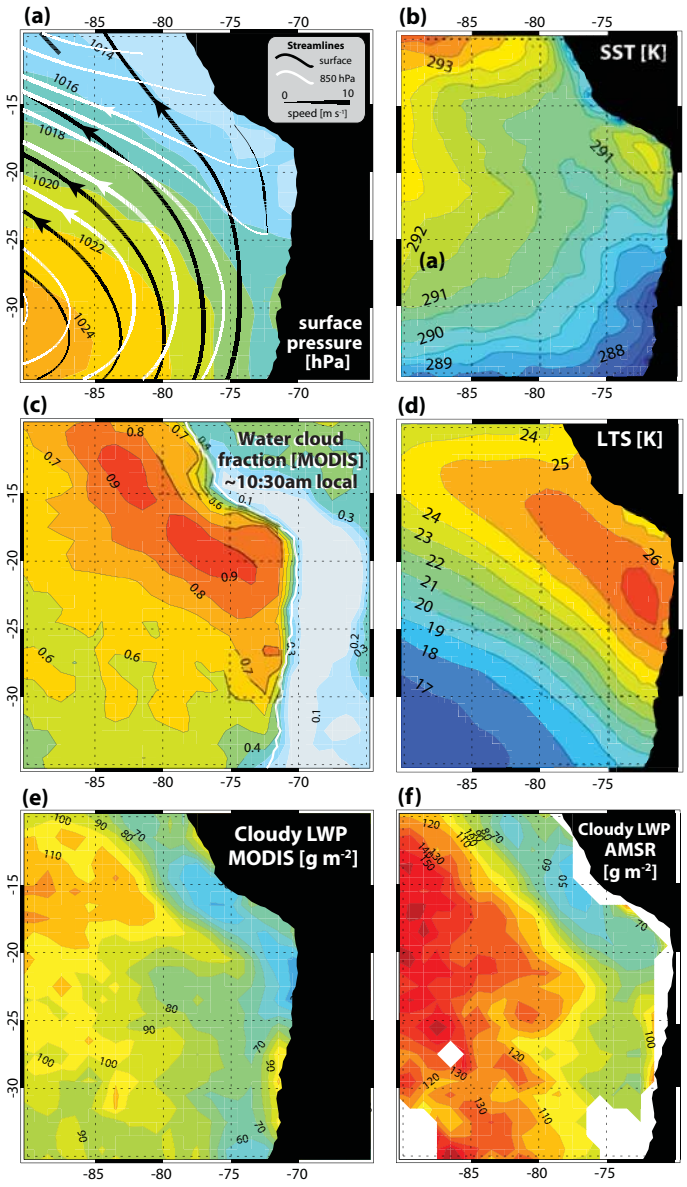

Figure 5: October-November mean values of (a) sea level pressure (colour contours) and flow streamlines at the surface (black) and at 850 hPa (white); (b) sea-surface temperature from the NOAA Optimal Interpolation analysis; (c) fractional cover of water clouds for October-November 2008 at 10:30am local time as determined by MODIS; (d) lower tropospheric stability (LTS, difference between potential temperature at 700 hPa and surface) from the ECMWF operational analyses; (e) mean LWP for cloudy pixels from MODIS; (f) mean LWP for cloudy pixels from AMSR (AMSR LWP/MODIS warm cloud fraction). In (e) and (f), we use the area mean diurnal mean LWP from AMSR (mean of 01:30 and 13:30 LT) divided by the mean warm cloud cover from MODIS, to provide an estimate of the cloudy sky LWP.

were 70 g m^{-2} or less.

Liquid water paths increase westwards, in agreement with in-situ observations (Bretherton et al. 2010). Still further west, the microwave-derived LWP estimates from AMSR increasingly exceed those from MODIS, which is indicative of increasing amounts of drizzle (see e.g. Shao and Liu 2004) formed in the thicker clouds of the deeper maritime MBL (Wyant et al. 2010, Zuidema et al. 2009).

While the mean flow illustrated in the previous section is somewhat representative of the observed day-to-day conditions in the MBL, in the FT variability on synoptic time-scales was very substantial.

The cloud-cover was observed to respond to the synoptic-scale variability of the circulation above the inversion to a degree such that the 48-hour operational forecasts of synoptic conditions could be usefully employed to estimate the expected changes in observable field conditions during the VOCALS-REx campaign. The model-generated cloud fields themselves provide a good guidance, in spite of the poor representation in the operation models of cloud microphysical processes or of aerosols.

In general, the main source of synoptic variability in the VOCALS-REx region was baroclinic activity in the jet-stream system, causing ridging and troughing in the FT which tended to be amplified by orographic effects near the Andes. This was associated with anomalous advection of air-masses from different latitudes or altitudes, following the ridging of the isoentropes.

When the disturbance was sufficiently strong, it developed into a coastally-intensified cyclone (Garreaud et al., 2001; Garreaud and Rutllant, 2003), most clearly seen in the lower FT at about 700hPa. In a few instances (e.g. 19-20 November), such coastal lows locally reversed the zonal component of the flow across the Andes to easterly, causing the advection of land air-masses into the maritime SEP area.

While anomalous cold or warm advection in the FT associated with these systems was common, occasionally regions at the low-latitudes of the VOCALS-REx area were directly interested by trailing cold fronts, with an ensuing sharp drop in FT temperatures. Such events appear to be more frequent on the eastern slopes in the lee of the Andes, but on 23-24 October such a cold front extended throughout the troposphere just above the MBL along 20S.

In addition, changes in the extent of the mid-tropospheric high, associated with changes in heating either from the elevated terrain of the Bolivian altiplano or from deep convection on the western and southern Amazon basin, caused modulations of the sub-tropical jet-stream on its equatorward flank which sometimes

appear associated with the formation of low-latitude cyclone waves.

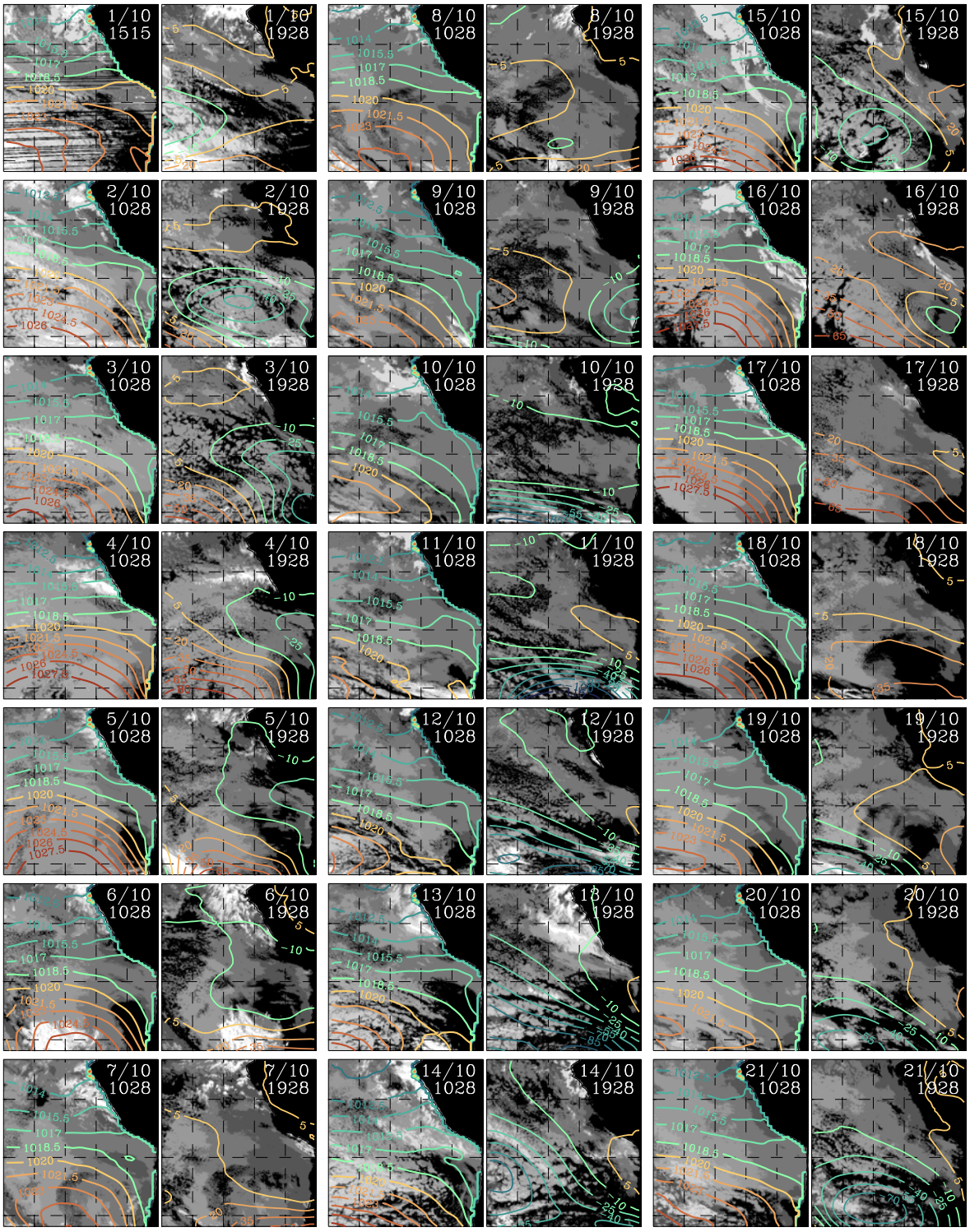
1/10 1515
1/10 1928
8/10 1028
8/10 1928
15/10 1028
15/10 1928
2/10 1028
2/10 1928
9/10 1028
9/10 1928
16/10 1028
16/10 1928
3/10 1028
3/10 1928
10/10 1028
10/10 1928
17/10 1028
17/10 1928
4/10 1028
4/10 1928
11/10 1028
11/10 1928
18/10 1028
18/10 1928
5/10 1028
5/10 1928
12/10 1028
12/10 1928
19/10 1028
19/10 1928
6/10 1028
6/10 1928
13/10 1028
13/10 1928
20/10 1028
20/10 1928
7/10 1028
7/10 1928
14/10 1028
14/10 1928
21/10 1028
21/10 1928

Figure 6: (Previous page). Twice-daily snapshots (where available, 10:28 UTC, i.e. 05:08 LT at 80°W, and 19:45 UTC, or 14:25 LT) of the temperature difference ΔT between the SST (as given by the daily-mean OSTIA product; Stark et al. 2007) and the GOES Channel 5 (12 μm) brightness temperature. Values of $\Delta T < 6$ K are black and indicate virtually cloud-free regions. All values above 35 K are considered to originate from high clouds and are marked in white. Gray colours indicate low clouds, with lighter shades generally indicative of higher clouds in deeper boundary layers. The contour interval for the shading is 3 K. The GOES data have been interpolated onto the 0.05 degree-square OSTIA grid, conserving areal averages. Superimposed on ΔT imagery are meteorological data from the Met Office global operation analysis. Overlaid on the night-time fields are sea-level pressure contours from the operational analysis for the previous 00 UTC. The contour interval is 1.5 hPa; the 1020 hPa line is drawn in light orange colour, and the 1018.5 hPa line in light cyan. On the day-time panels, contours of the zonally asymmetric part of the 500 hPa geopotential height field are drawn, for 00 UTC following the image. A contour interval of 15 m is used, with positive values (at and above 5 m) in orange/red, and negative values (at and below -10 m) in cyan/blue.

4.2 Day-to-day variability in October and November 2008

The general meteorological conditions for the period of interest are shown in Fig. 6. For each day, we show the cloud field using the difference ΔT between the SST (as given by the daily-mean OSTIA product; Stark et al. (2007) and the GOES Channel 5 (12 μm) brightness temperature. Since few low cloud tops occur below 600 m in the region (e.g. Zuidema et al. 2009), all values of $\Delta T < 6$ K are left in black to indicate virtually cloud-free regions, while all values above 35 K are considered to originate from high clouds and are marked in white. The lower threshold is still somewhat problematic because differences less than 8 K can still indicate either low, continuous cloud cover, or fields of broken cumulus with relatively high cloud tops. Comparison with GOES-10 day-time images in the visual band generally supports the choice made, and broken cumulus fields tend to be infrequent in the VOCALS-REx study area. We show this temperature difference field twice-daily: (a) during early morning before sunrise (where available, 10:28 UTC, i.e. 05:08 LT at 80°W), when the cloud cover is most extensive, and (b) in the afternoon (19:45 UTC, or 14:25 LT at 80°W) when the clouds are near their thinnest (Wood et al. 2002), and on many days the stratocumulus deck partially

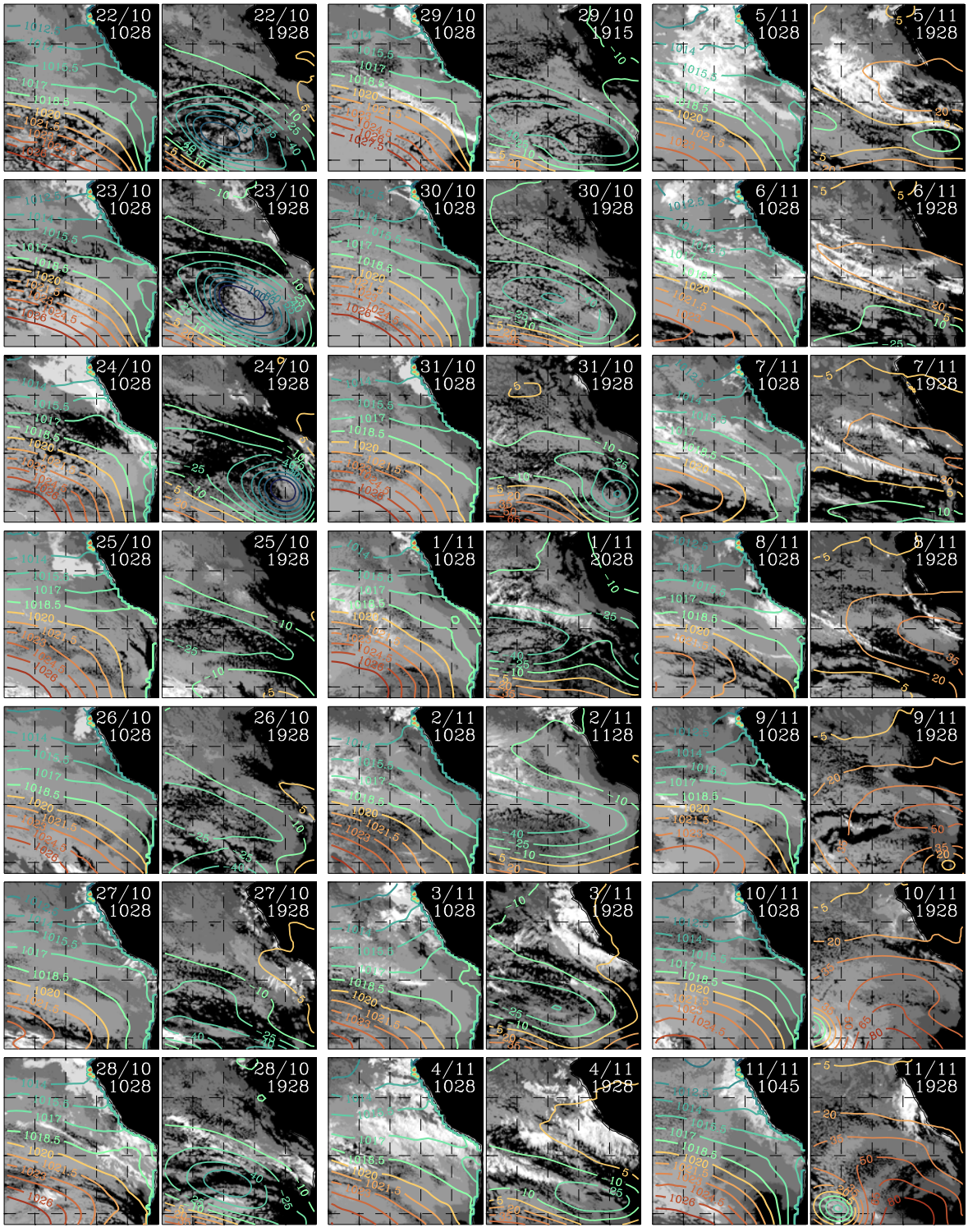

Figure 6 (continued)

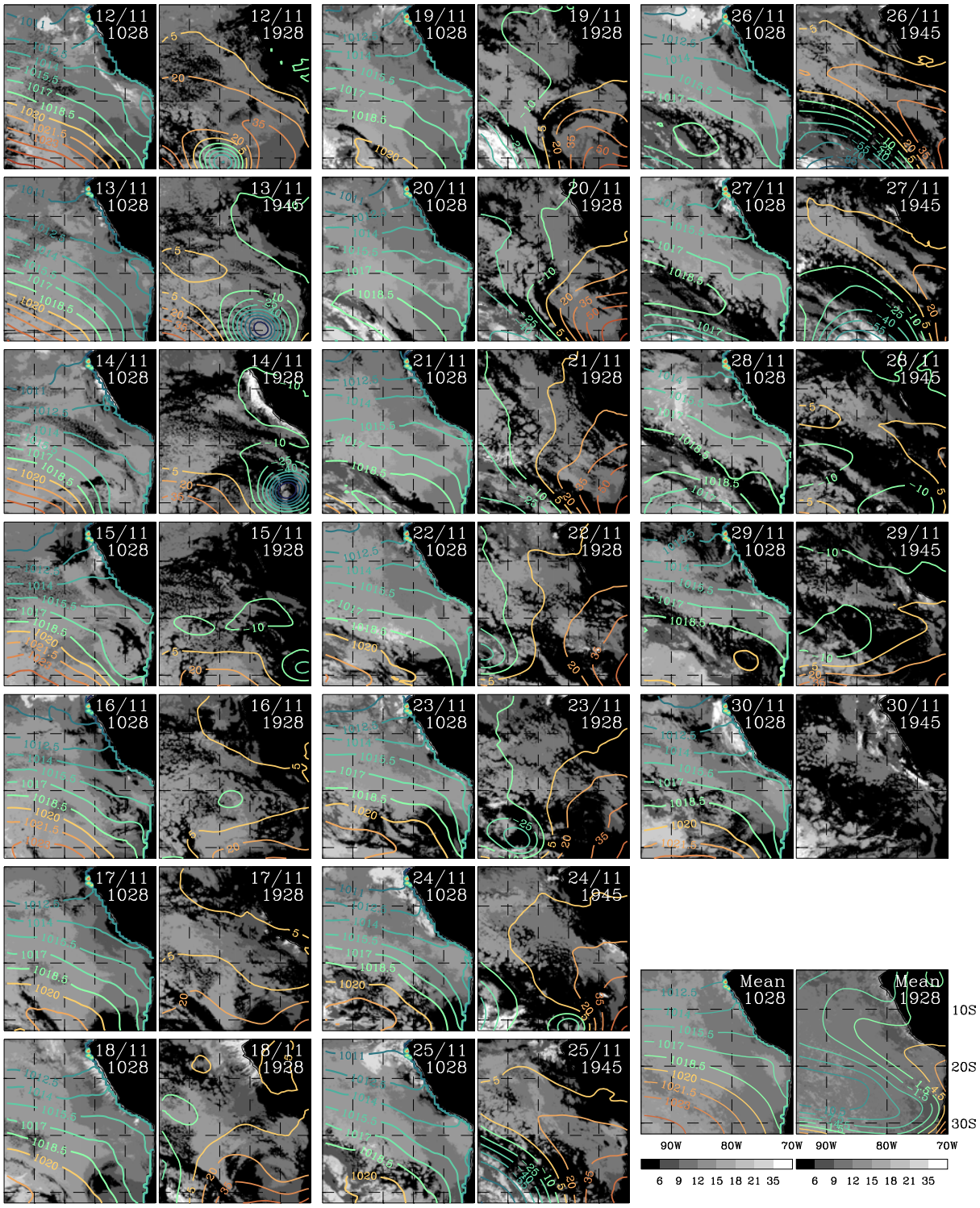

Figure 6 (continued) The final two panels show the October-November mean values of ΔT when cloud is present (determined as being when $3 < \Delta T < 35$ K) for the morning and afternoon times, with contours of mean pressure (overlaid on morning) and 500 hPa geopotential height (afternoon).

breaks up (Rozendaal et al. 1995, Bretherton et al. 2004, Abel et al. 2010).

Superimposed on the night time ΔT fields in Fig. 6 are sea-level pressure contours for the previous 00 UTC, and on the day time field contours of the zonally asymmetric part of the 500 hPa geopotential height field are drawn. The final two panels in Figure 6 show the average night-time and day-time cloud-top temperatures at each location whenever low cloud is diagnosed (i.e. whenever ΔT is within the stated thresholds of 6 K and 35 K), with contours for mean pressure and 500 hPa height overlaid as before.

We discuss here two important aspects of the variations in the cloud field in the VOCALS-REx region. Day-to-day variations in the cloud fields are comparable to diurnal variations, and in some cases dominate. These synoptic changes occur in coincidence with changes in sea-level pressure and the passage of mid-tropospheric synoptic-scale disturbances. In particular, there is a strong association between low 500 hPa heights and cyclonic flow at 500 hPa, and large-scale clearing and breaks in the cloud cover, particular towards the south of the VOCALS-REx study region. This is particularly evident when synoptic systems approach the South American coast (e.g. October 1-3, October 10-13, October 20-25, November 12-15, and after November 24). Equally remarkable are the intervening episodes of synoptic ridging, particularly during October, which coincide with increased Sc cloud-cover.

Superimposed on this distinctly synoptic variability, circulation-related anomalies can be observed at both smaller and larger spatial and temporal scales. Near land, enhanced orographic subsidence associated with synoptic-scale ridging is responsible for sudden, strong coastal clearings.

This is accompanied by a localised reduction in sea-level pressure and formation of a coastal low (CL), as discussed in Garreaud et al. (2002). The coastal clearings typically persist for up to 3 days after the initial mid-tropospheric ridging, and they tend to be located in the southern part of the domain of interest here, where the coastal jet is strongest, consistent with the dynamics discussed by Munoz and Garreaud (2005). Such "canonical" CLs are seen to occur during October 4-5, October 17-18, and November 10-11.

The association between mid-tropospheric ridging and sea-level troughing along the coast distinguishes CLs from mid-latitude synoptic disturbances (Garreaud et al. 2002). Nevertheless, their character is thought to depend principally on the interaction of synoptic-scale disturbances with the mountain topography, whereby changing up- and down-slope flows affect the temperature and moisture stratification of the lower atmosphere near the coast, thereby affecting the pressure field. These changes also affect the cloud-

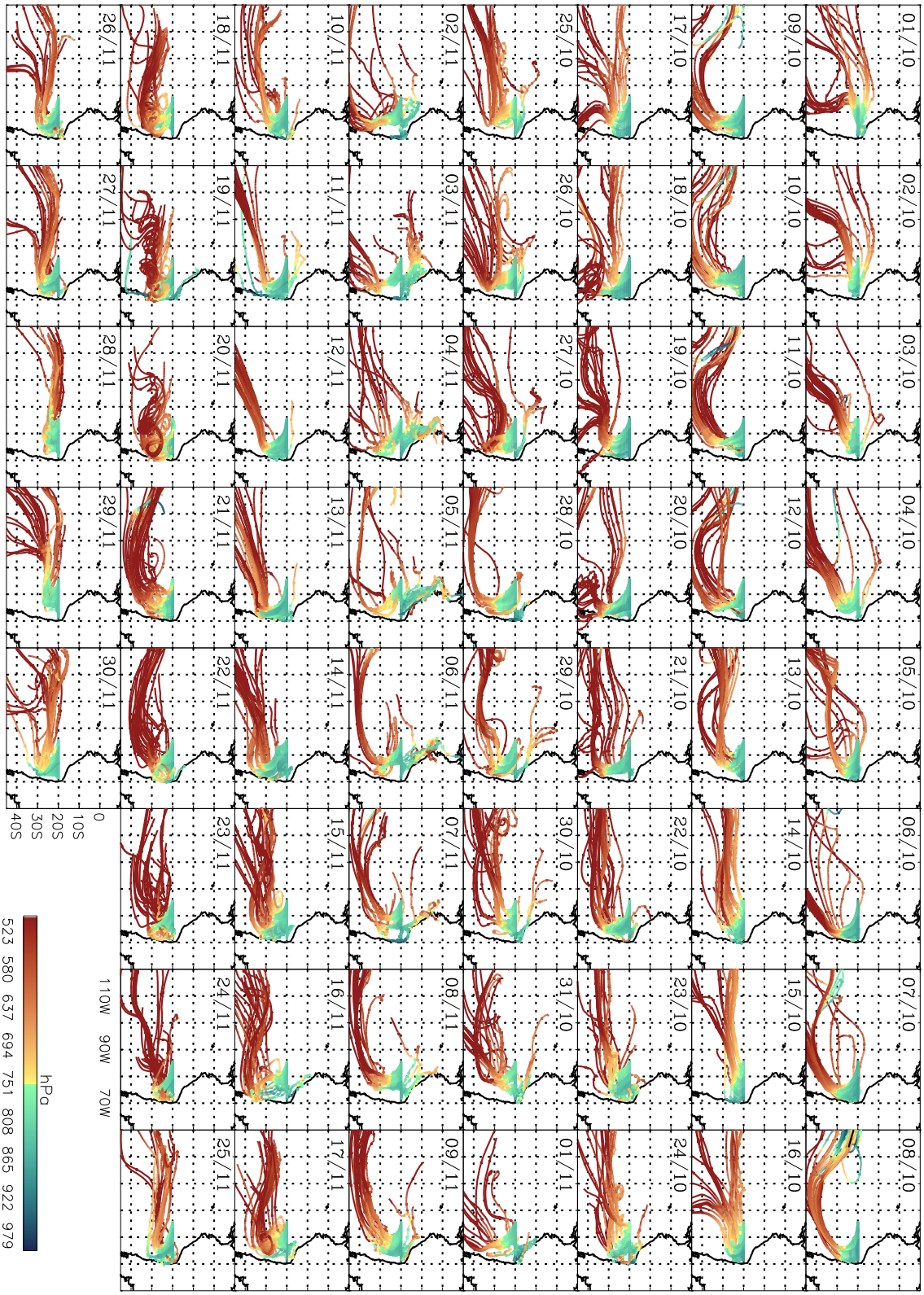

Figure 7: Ten-day back-trajectories of air reaching 20S between 72W and 85W at a lavel between 20 and 40 hPa above the inversion at 00UTC for each day of October and November 2008 on 23 October 2008. Colour-coding shows the pressure at each point of each trajectory (scale at the bottom). Many trajectories extending zonally along the mid-latitude jet-streams are only visible in their initial portion. The back-trajectories are calculated

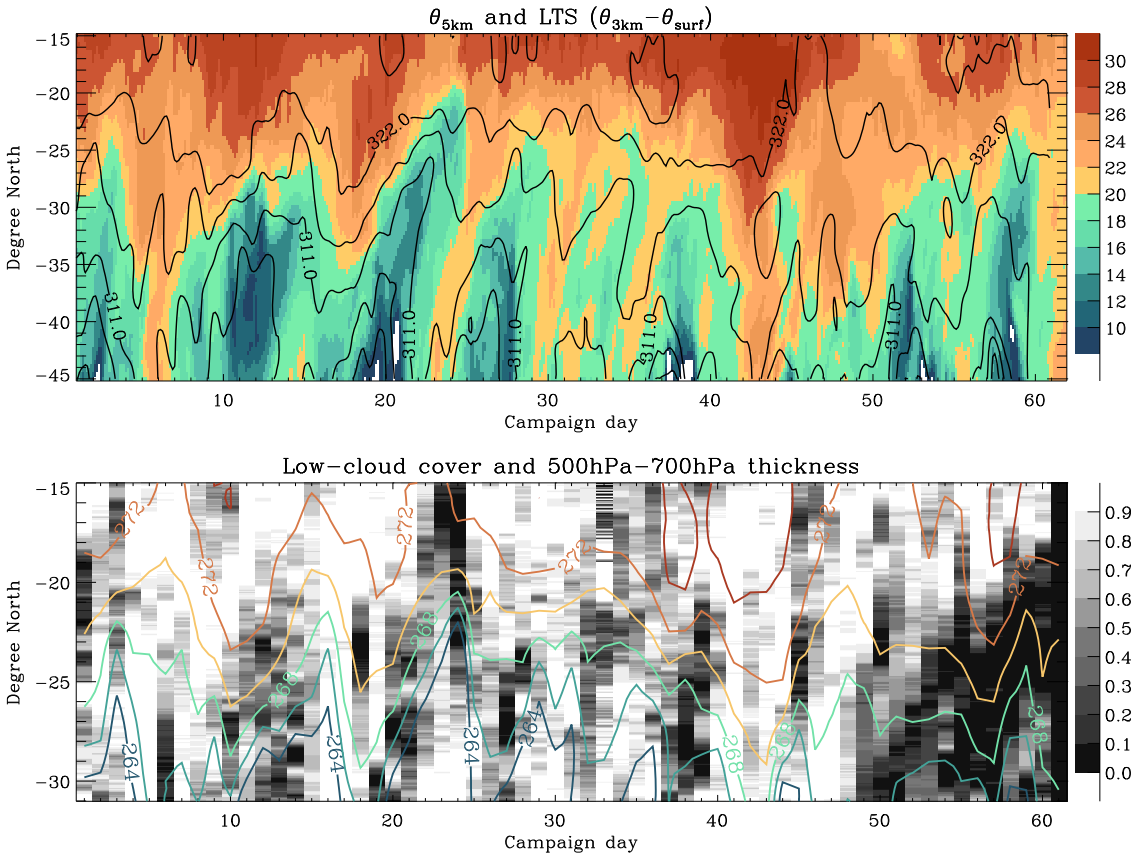

Figure 8: (a) Lower tropospheric stability ($\theta_{700} - \theta_{surf}$) averaged over 80-85°W, as a function of time and latitude; (b) as (a) but for cloud fraction from GOES at 19:30 UTC (late afternoon), and 500-700 hPa thickness contours. Thickness and temperature data from UKMO global operational analysis and 3h-21h forecasts.

cover. Thus, on the one hand, CLs depend on the presence of large-scale ridging and troughing. On the other hand, height anomalies associated with synoptic disturbances generally tend to assume a baroclinic character as they interact with the orography, and to disturb the coastal cloud field in a way consistent with the associated mountain winds.

Thus, there are instances - such as November 1-2 - of weak coastal troughing and of ridging at 500 hPa height, which area hardly accompanied by sea-level changes, but nonetheless affect the cloud field, sometimes quite significantly (e.g. November 7-9). This particular extensive cloud-clearing event is still associated with mid-latitude troughing further south (at the southern edge of the VOCALS-REx study region), but also with

strong warming of the mid-troposphere overlying the coastal ocean north of about 25°S, that appears to emanate from the continent to the east. This results in an enhanced mid-tropospheric meridional temperature gradient, and strong cold advection over the southern half of the domain (see Fig. 8).

The importance on the regional scale of synoptic ridging and troughing near the coast also concerns the origin of the air-masses, and their accompanying aerosol or pollutant load, that were sampled in the SEP area during the VOCALS-REx campaign. The back-trajectories arriving near the inversion along 20S during VOCALS-REx, shown in Figure 7, highlight two particular episodes during which air-masses were advected towards the Sc closer to the coast (typically, within 5 degree in longitude) from potentially polluted land areas. The first such episode occurs in Oct 17-21, following an intense synoptic troughing and subsequent ridging along a NW-SE axis to the south of the VOCALS-REx area. The corresponding turning of the geopotential height countours implies advection from the central and southern portion of the Chilean land-mass. Over 20S, the riding peaks on 17 October and coincides with a shallow MBL and persistent, continuous cloud cover. A weaker, but similar occurrences is seen on 16 November, also corresponding with a depressed MBL and increased cloud-cover along 20S. Such episodes roughly represent an intensification of the anticyclonic circulation south of the VOCALS-REx area which may be brought about by synoptic ridging.

A distinct dynamics appears to be associated with the second period when air-masses are potentially influenced by land areas, spanning roughly two weeks between the late part of October and the early part of November, but with increased relevance between 3 and 8 November. In this period, air-masses near the coast originate from the North, and appear to come in contact with Peruvian and Ecuadorean coastal land areas. From 23 October onwards increased occurrence of cirrus is observed north of 20s, becoming particularly marked during 3-6 November. Likewise, mid-tropospheric relative humidity is markedly higher than during the rest of the season. During this time, the Bolivian mid-tropospheric anticyclone appears to intensify and extend westwards over the maritime area around 15S. After 10 November, it becomes detached from the continent and appears to move westwards, possibly as a free planetary wave, until it is dissipated around 14 November. This evolution is accompanied by a significant warming of the free-troposphere over 20S.

To some extent, the back-trajectories of air reaching 20S between 5 and 7 November highlight the circulation in this mid-tropospheric anticyclone. It is interesting to speculate on the possible role of convection over

the Amazon and adjacient land. Increased moist convection there and over the Mato Grosso is suggested from satellite OLR maps in the period 18-20 October, and again later between 30 October and 3 November. Such episodic thermal forcing of the mid-troposphere may well excite travelling Rossby waves as suggested above. The anomalous upper-level circulation brings tropical, continental air in the vicinity of the MBL in the SEP, in sharp contrast with the usual remote oceanic and subtropical air-mass origin there (Grant et al. 2010). Given the persistent, strong easterly outflow over the low-lying coastal areas of Ecuador, one cannot exclude, in principle, a remote origin from the Amazon basin for some of the air. Whether continental pollution of SEP air-masses induced by events like these may have been relatively under-represented during the VOCALS-REx campaign, as South America was anomalously dry compared with climatology (see Figure 19), is an open question.

Dynamical processes at sub-synoptic scales, as discussed e.g. by Munoz and Garreaud (2005), are locally always important near the coast, for example where an approaching mid-latitude disturbance appears to be associated with the development of a distinct coastal anomaly ahead of it (e.g. October 22-23). Similarly, during November 15-16, following the passage of a mid-tropospheric cyclone across the Andes, a rapid drop in pressure along the coast coincides with extensive coastal clearing. For reasons both of resolution and imperfect representation of the terrain, this dynamics is not captured by either global or regional forecast models (Wyant et al. 2010, Abel et al. 2010), which all appear to miss the coastal cloud anomalies (along with much of the diurnal cycle there). However there is a clear indication from trajectories that become "entangled" with such events that they may considerably prolong the residence time of air-masses above the MBL along 20S.

Variability that appears associated with a longer temporal scale is most apparent in the second half of November.

From November 19 onwards, a persistent north-westerly anomaly is seen at 500mb (Fig. 6). This feature corresponds to west-north-westerly total mid-tropospheric flow throughout this period, corresponding to a large-scale cyclonic anomaly over the ocean to the west of South America. In spatial coincidence with the strongest poleward flow, reduced large-scale subsidence is diagnosed from the forecast model, consistently with vortex stretching. In the same areas, the day-time cloud images show a band of clearing. The low-pressure centre to the west is part of a slowly evolving wave-train that spans the south-Pacific basin, and

appears to emanate from the Maritime Continent, in association with a positive phase of the Madden-Julian Oscillation (MJO), as shown in Section 7.

During much of the month of October 2008, changes in cloud cover generally follow a succession of synoptic disturbances travelling through the region, with similar effects during the day and during the night. Cloud cover is generally high, with relatively small differences between night and day (in a few instances even negative over the oceanic area west of 82°W), but is characterised by rapid, near-complete clearing in large, dynamically well-defined areas, dominated by cyclonically turning mid-tropospheric flow, where a combination of cold advection and negative-vorticity advection occur.

Later in the Spring season, from the end of October to the middle of November, diurnal variations in cloud cover are larger, and on sub-synoptic time-scales coastal and other smaller-scale clearing events (such as those associated with pockets of open cells) become m ore important. During this period, there is little synoptic activity from mid-latitude depressions, the cloud cover is nearly complete during night-time, while the day-time break-up, while variable, is never very large, except on November 8 (as discussed above).

As a rough conceptual schematics, one might summarise the previous discussion by dividing the whole of October-November 2008 into three distinct periods. The first period, until the end of October, has robust synoptic activity from mid-latitude depressions which largely control the cloud conditions. The second period, in the first half of November, shows reduced baroclinic activity, with high values of sea-level pressure, and sub-synoptic scale activity, including influences from continental convection, on time-scales of 2-3 days. The third and final period has moderate synoptic variability, and is dominated by a large-scale circulation anomaly which reduced mid-tropospheric subsidence and allowed for an extensive day-time break-up of the stratocumulus.

Away from the relatively narrow coastal strip, cloud-free areas tend to be zonally aligned and to propagate northwards with the boundary-layer flow. This may be partly due to a memory of the air mass, which being depleted of CCN once a closed to open cell transition involving precipitation occurs (see e.g. October 27/28 case study of Wood et al. (2010) and associated modelling work by Wang et al. (2010) and Berner et al. (2010)), remains so for a length of time. However, at the latitudes most relevant for VOCALS-REx, synoptic disturbances themselves also tend to travel equatorwards as they approach the barrier of the Andes (see Fig. 8).

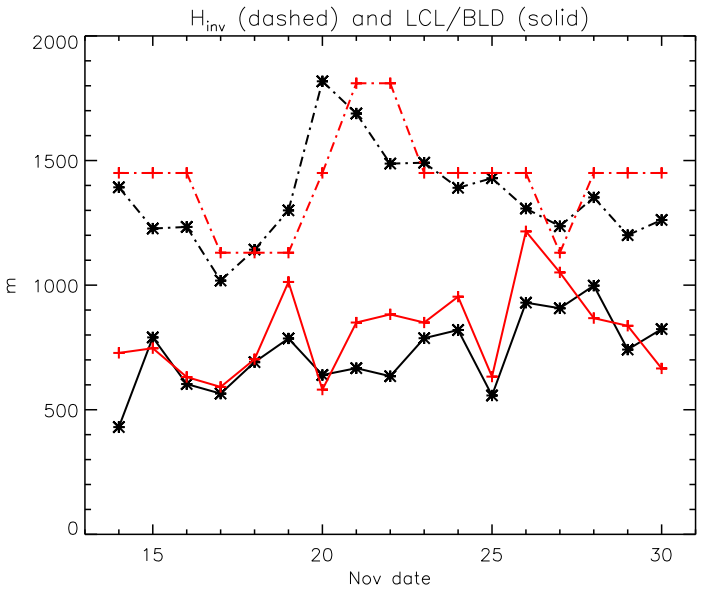

Figure 9: Inversion height and LCL as estimated from data from R.H.Brown radiosonde launches (black lines), and diagnosed from the UKMO operational forecasts (red lines).

5 Depth of the MBL and variability in oceanic cloud cover on synoptic time-scales

The operational forecast model of the UK Met Office produces cloud fields which compare well with satellite-derived products in open-ocean areas (Abel et al. 2010, see their Figure 5). Averaged over the area between 90W-80W and 15S-25S, the model-derived daily-average low-cloud cover has a correlation of 0.78 (60 points) with that derived from GOES-10. (An identical correlation is found for averages restricted to the zonal strip 90W-75W, 19.5S-20.5S). We also diagnose an MBL-depth from the model fields, by the level of the MBL-capping inversion (the inversion height, h_{inv}). This quantity has a weaker correlation of -0.60 with GOES-10 cloud-top brightness temperatures. The biggest discrepancies occur in late October and early November, when contamination from cirrus cloud (see Figure 6) imply that GOES-10 broad-band IR radiances images do not always reliably represent the Sc top. A good agreement is found between the model-derived h_{inv} and a similarly defined quantity from the profiles returned by ship-based radiosonde ascents (Figure 9).

The model-diagnosed total low-cloud cover and the inversion height are strongly and negatively correlated

(Figure 10). In general, reduce cloud-cover tends to be associated with elevated cloud-tops, i.e. deep MBLs. As indicated from Figure 10, direct measurements show a similar correlation. It should be noted that day-to-day variations in cloud cover are most pronounced during daytime, in such a way that the diurnal average cloud cover and its diurnal range are strongly anticorrelated (c.c. around -0.9 on both model-derived and satellite-derived estimates). In general, areas of clouds with shallow MBLs (low ΔT) during night-time tend to undergo less day-time break-up. A similar relationship is found with surface solar irradiation.

Figure 10 also highlights the different character of the three periods identified in the previous section. Until the end of October, cloud-top heights are very variable, with characteristic synoptic temporal and spatial scales. The early part of November, up to the 15th, is generally characterised by low cloud-top heights, especially towards the end; while the second half of November sees higher cloud-tops, prone to day-time break-up. The averages in the area 90W-75W, 19S-21S are 1569m, 1461m, and 1587m for h_{inv} for the periods October 1-31, November 1-15 and November 16-30, respectively. Correspondingly, the model-derived fractional cloud cover is 0.72, 0.80 and 0.60, respectively; the satellite-derived values are 0.75, 0.78 and 0.56, respectively. It thus appears that, over maritime areas, lower inversion heights do generally correspond with increased cloud-cover. A similar statistical correlation was found in MODIS-derived data by Wood and Hartmann (2006; see also George and Wood, 2010). In coastal areas, observed variations in cloud-top height are smaller and less well correlated with cloud cover. The effects of a strong mean diurnal cycle are also more significant in that region (see Section 8). Since the model performance is much weaker on and near land (Abel et al. 2010), we limit our considerations in this section to maritime areas well offshore (more than 300km from the coast).

The UKMO operational model has no representation of cloud-aerosol interaction, and a very rudimentary parametrisation of cloud-microphysical effects. Moreover, its horizontal resolution cannot capture the effect of precipitation on mesoscale dynamics in the MBL. The model does not have any representation of mesoscale or smaller features, including for example the development of pockets of open cells. Thus, its qualitative consistency with observations in both MBL-depth and cloud-cover is non-trivial. Although the model tends to dissipate some cloud with increasing forecast lead time, the simulated day-to-day variability is not solely or primarily due to assimilation increments. Initialised free-running simulations of the model in one of its climate configurations, HiGAM (Shaffrey et al., 2009), show an evolution of the cloud field in the SEP

that remains very close to the operational analyses for up to 10 days. Therefore, the UKMO operational forecasts represent a valuable opportunity to isolate the effects of dynamical forcing on the Sc field in the VOCALS-REx region.

In this model, an elevated inversion consistently corresponds with increased areal cloud fraction if averages over a sufficiently large area and away from land are considered. Figure 10 highlights variability with a typical synoptic time-scale of about a week or less. However, over the observations period there is no clear indication that this correlation breaks down on longer time-scales. Smoothing the two time-series in Figure 10 still results in formally significant correlations. Nevertheless, it appears that large-scale circulation anomalies not associated with synoptic-scale systems, which affected VOCALS-REx in the second half of November, when cloud cover was considerably reduced, do play a role. It is apparent, also, that especially intense synoptic events, such as that occurring in October 22-24, are more than proportionally effective in reducing cloud cover, leaving a signature on longer time-averages. This acquires particular significance when considering the similarly skewed relationship between cloud cover and surface insolation.

Figure 11 shows the mid-tropospheric circulation anomalies associated with changes in the inversion height in the area 90W-75W, 19.5S-21.5S (indicated by the black rectangle). The composites based on the inversion height, h_{inv}, extrema shown in Figure 10 indicate that negative (positive) inversion-height anomalies (with positive/negative cloud-cover anomalies) coincide with anomalous warm (cold) advection in the lower FT within anticyclonic (cyclonic) synoptic disturbances when they approach the area of interest. Vertical sections in the meridional plane of these events (not shown) confirm a baroclinic structure, with descent (ascent) associated with a tilted warm (cold) front. Linear correlations with h_{inv} (not shown) show a very similar, formally significant structure. As may be expected, the associated temperature advection is most intense in the lower free-troposphere just above the MBL.

It appears from Figure 11 that the cold frontal systems tend to coincide with cyclones at low latitudes, around 30S, as they approach the Andean barrier, while the warm fronts tend to occur in association with extratropical storms south of 40S. Composites based on the storms themselves (not shown) as they occurred during the period of interest confirm this impression. The leading term in the heat advection anomalies is associated with anomalous vertical motion. Figure 11 suggest anomalous ascent near the Andean topography associated with synoptic troughing, and anomalous descent associated with synoptic ridging. Note also the

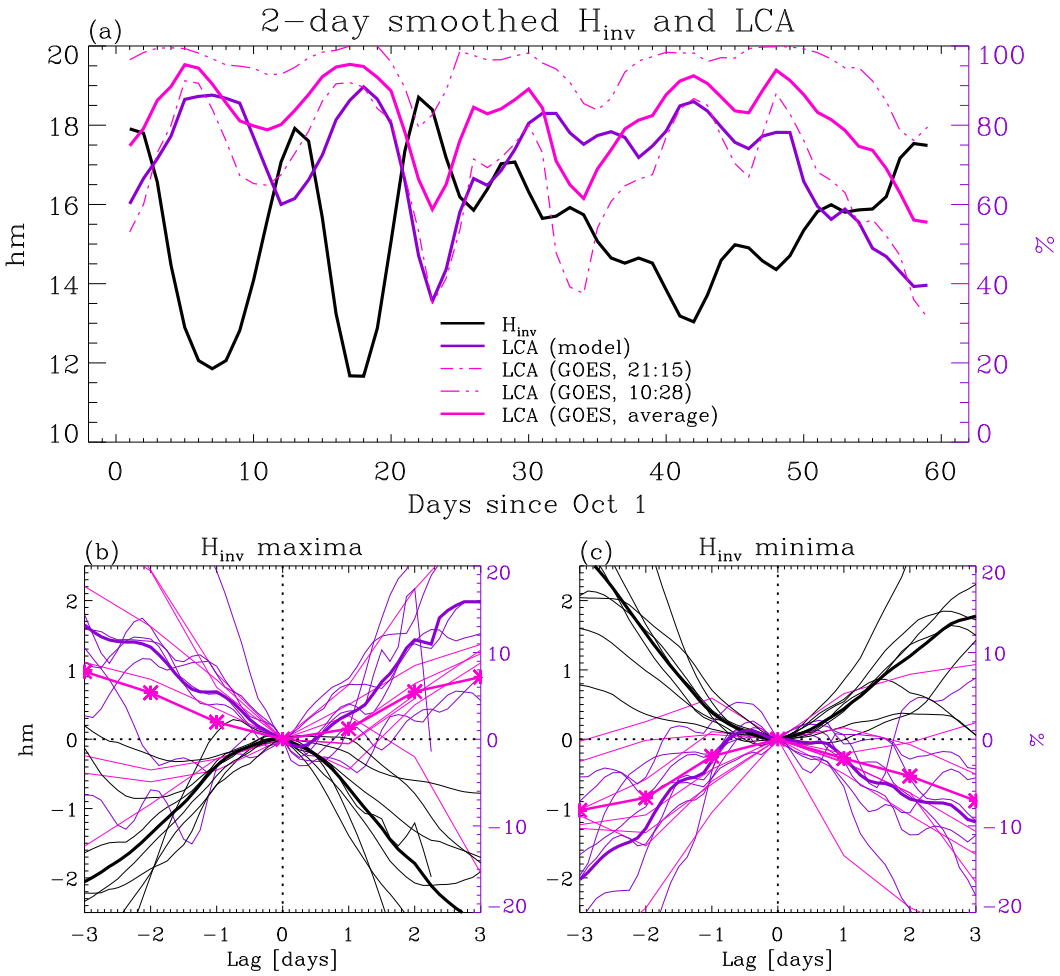

Figure 10: *(a)*: UKMO model-simulated inversion height (full black line) and low-cloud cover averaged over the region 90W-80W, 15S-25S. Both model-derived and satellite-derived (GOES-10) low-cloud cover are shown, in violet and magenta colours, respectively. The thin broken lines show the satellite-derived daily minima and maxima. *(b) and (c)*: composites of inversion height and cloud cover in the region 90W-80W, 15S-25S based on the extrema of the daily-average MBL depth averaged over 90W-80W, 19.5S-20.5S.

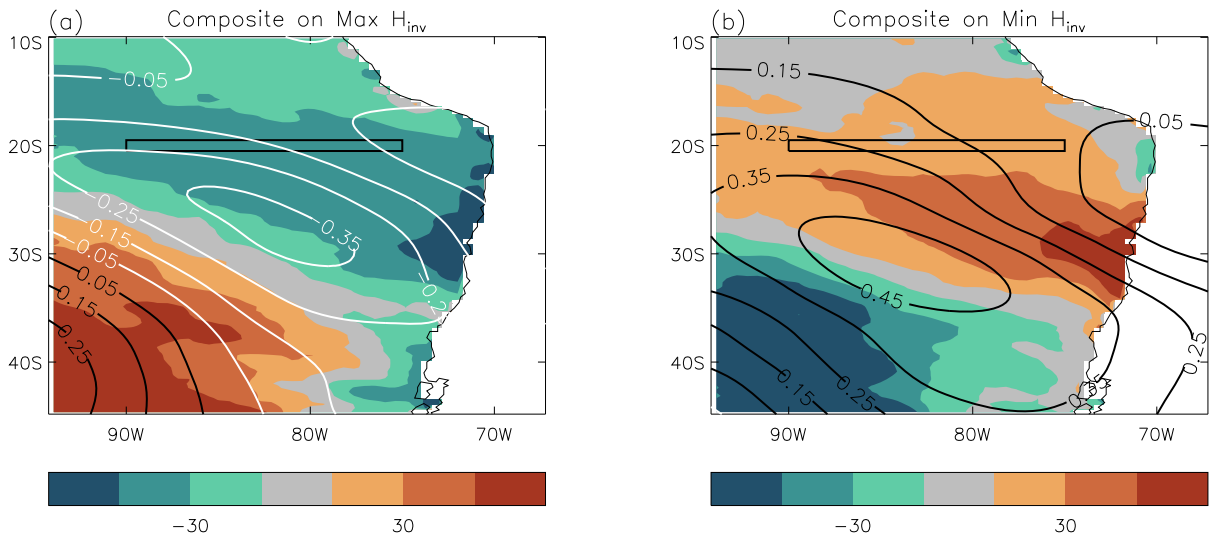

Figure 11: Composite maps of 50hm streamfunction anomalies and vertically integrated temperature advection in the FT above the MBL for the positive (panel (a)) and negative (panel (b)) extremes in inversion height, h_{inv}, shown in Figure 10. The maps show average anomalies over 48 hours prior to the extrema in h_{inv}. Colour-coding refers to heat advection (units are J m^{-2} s^{-1}; 100 J m^{-2} s^{-1} roughly correspond to 1 K/day mass-averaged anomalous temperature tendency in the FT. Coutour lines show the streamfunction anomalies, in units of Mm^2 day^{-1}. Positive values, marked by black contours, correspond to anticyclonic circulation (apparent in panel (b)), and negative values for cyclonic circulation. Data from operational analyses and 3h-21h forecasts are used.

association of the latter with advection towards 20S from land areas to the South (cf. discussion on Figure 7 in the previous section). These results are consistent with the analysis of Xu et al. (2005) who find that anticyclonic circulation anomalies which tend to reinforce the climatological zonal pressure gradient and generate offshore flow in the lower troposphere off the Chilean coast tend to increase cloud-cover while depressing the inversion and represent an important mechanism in the generation of subseasonal variability in the Sc deck. In our composite the anticyclonic anomalies also appear to have a more stationary character than the rapidly evolving cyclones, while the latter are associated with the largest vertical wind anomalies.

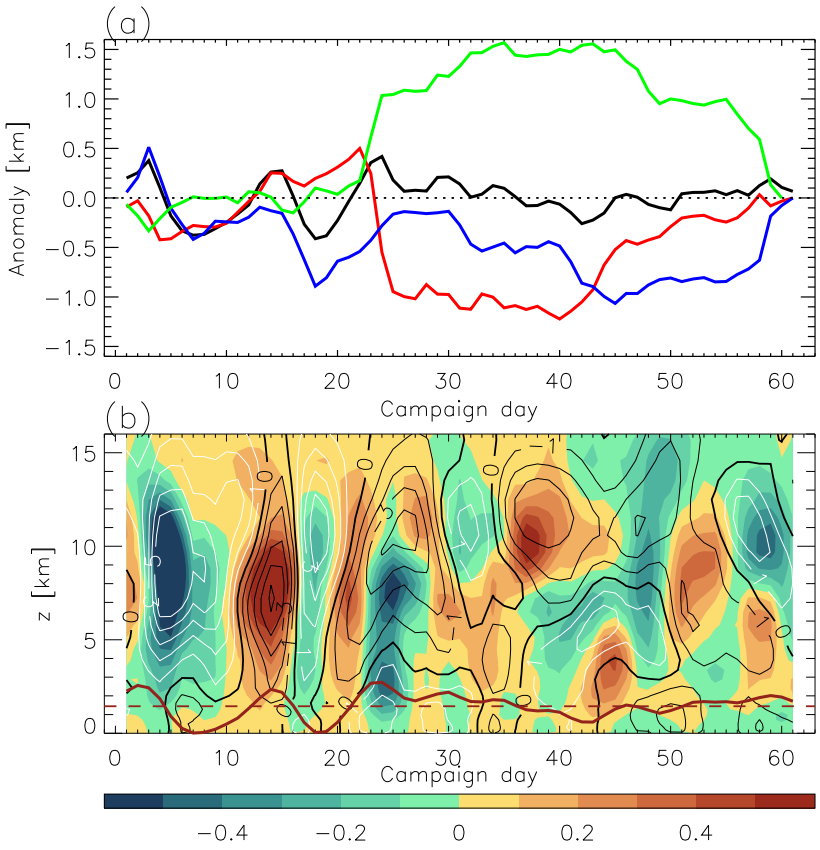

Figure 12: (a) Time evolution of the 90W-80W, 20.5S-19.5S average inversion height (solid line), compared with the evolution implied by the partial tendencies associated with changes in the vertical velocity only (red line), in horizontal advection only (blue line), and in the residual, interpreted as entrainment (green line). The time-mean values of the partial tendencies were removed. (b) Height-time Hovmueller diagram for the 90W-80W, 20.5S-19.5S area average meridional (contour lines) and vertical (colour-coding) mass-flux for October-November 2008. Contour interval is 0.5 kg/m^2/s for the meridional component, and 0.5 g/m^2/s for the vertical component (the transition from cyan to yellow marks the zero line). The height of the inversion is indicated by the dark-red line, the excursions from the mean being exaggerated 3-fold for clarity. A 2-day smoothing is applied to all quantities. Data are from the operational analyses for the inversion height n panel (a), and from both analyses and 3h-21h forecasts for all other quantities.

In general, the height tendencies may be decomposed into a part due to vertical advection, a part due to horizontal advection, and a part due to entrainment, the latter being diagnosed as a residual according to

$$\dot{m}_\epsilon/\rho = \partial_t h_{inv} + u \cdot \nabla_2 h_{inv} - w\,, \tag{1}$$

where all quantities are calculated for $z = h_{inv}$. Here, $\dot{m}_\epsilon$ represent the entrainment flux, u the horizontal wind, and w the vertical wind. This decomposition, shown in the thin lines in Figure 12, shows a dominant contribution for the inversion height tendencies the area 19.5S-20.5S,90W-80W by the horizontal advection of height anomalies in the first period of the campaign (October 1 to October 27), to be later partly replaced by a contribution from vertical velocity anomalies. These results are consistent with those of Rahn and Garreaud (2010b), who perform a similar analysis, and demonstrate that horizontal advection gives the leading-order contribution to changes of the MBL depth over synoptic time-scales. As a comparison with Figure 11 suggests, we find that vertical advection anomalies become markedly more important near the coast, especially to the South, i.e. upstream, of 20S. Thus, temperature anomalies in the lower free-troposphere that are generated by the interaction of synoptic system with the orography are communicated downstream via horizontal advection.

In general, atmospheric heat advection is dominated by the vertical and meridional components, which partially counteract each other. Panel (b) in Figure 12 highlights the dynamical relationship between vertical velocity anomalies and anomalies of the meridional flow. Initially, a sequence of upper-level wave cyclones invest the area, with mid-tropospheric ascent and descent associated with poleward and equatorward flow, respectively. On October 22, a mature baroclinic system marks the transition to a period with reduced synoptic variability but marked activity by baroclinic planetary waves, in which vertical motion is more strongly associated with the conservation of planetary vorticity. At the level of the inversion, the different character of the evolution between the three periods is seen clearly in panel (b) of the Figure. In early November, the induced motion is downward, to switch to anomalous ascent later.

The term in the vertical velocity in Equation 1 suggests the vertical displacement of a material surface, and horizontal advection near the inversion appears as the advection of MBL-depth (inversion-height) anomalies. Such a picture, however, is misleading. Due to the occurrence of cloud-top entrainment necessary to maintain mass continuity between the large-scale subsidence in the free troposphere and the divergent anticyclonic flow in the MBL, the inversion does not behave like a material surface, or as an isoentropic surface. On synoptic

time-scales and shorter, adiabatic processes, i.e. advection, dominate the tendencies in potential temperature in the lower FT. MBL temperatures, on the other hand, are closely tied to the more persistent SSTs. The fastest process at hand is represented by diabatic turbulent entrainment across the inversion that controls the location and the structure of the cloud layer. We therefore hypothesise that the mechanism responsible for reduction (increase) in cloud cover with increased (reduced) MBL-depth is increased (reduced) entrainment across the inversion that occurs with in response to a cooler (warmer) lower free-troposphere. Entrainment, as diagnosed from the residual of Equation 1, indeed generally counteracts the tendencies associated with advection. On short time-scales entrainment also correlates with the amplitude of the diurnal cycle in cloud cover, as the main mechanism for cloud destruction. High-pass filtering the time-series of daily values with a 4-day cut-off gives a weak but still significant correlation of 0.3 with the difference between daily maximum and daily minimum cloud cover. On longer time-scales, periods with increased cloud cover also tend to have higher entrainment.

The homogenisation in wet-bulb potential temperature that is seen across the inversion layer in both the model vertical profiles and in radiosonde ascents (not shown) supports the view that the occurrence of buoyancy reversal (e.g., Deardorff 1980) is instrumental in determining subseasonal variations in cloud-top height in the presence of strong free-tropospheric subsidence.

We elaborate on this further. The thermodynamic profiles of the lower atmosphere appear to control the level of the inversion, as it is usually observed to occur at or immediately below the level where the wet-bulb potential temperature reaches a minimum. This result appears confirmed by radiosonde measurements taken from the R.H.Brown research vessel during VOCALS-REx. A natural interpretation for such behaviour is for the inversion to be located where conditions are favourable to cloud-top entrainment mixing, and the concurrent thickening of the MBL can act to balance the divergent surface circulation in the anticyclone.

The location of the minimum in the vertical profile of θ_w may be approximately reconstructed from the profiles of θ that are characteristic for the mean FT and the mean MBL. In the FT, θ increases with height, as it does in areas of tropical deep convection with which the subtropical anticyclone is dynamically and advectively connected. Radiative cooling ensures that in the upper FT the temperature profile is slightly steeper than in the deep-convecting tropics; but lower in the FT (below 5000m), the lapse rate deviates very little the from tropics-wide average. In the MBL, θ is constant up to the cloud base, while in the cloud

layer θ_w is approximately constant. The point of intersection between the two resulting profiles of $\theta_w(z)$, decreasing in the MBL, and increasing in the FT, may be thought as marking the location of the MBL-top inversion. From these premises one may thus expect that a warming of the MBL, or a cooling of the lower free troposphere, will cause the MBL depth to increase; and conversely.

We thus suggest a general argument for the maintenance of a nearly vanishing jump in $\theta_w(z)$ at the inversion, and thus on its location and the variability thereof. Its implication may be formulated in terms of the LTS diagnostics (Figure 8), consistently with the known correlation between reduced cloud cover and a lower LTS (George and Wood 2010). To some extent, higher LTS can simply reflect the deeper MBL occurring with a cooler lower FT. However, the same jump in RH at constant θ_w does correspond to a smaller jump in dry stability when the temperature is lower, so that higher MBL tops correspond to less stable inversions. This correlation is robustly represented in the operational analysis data.

The assumption under which this argument may hold is that the spatial and temporal scales considered are large enough for an approximate equilibrium, but also small enough that the large-scale constraints on mass and energy conservation remain unchanged. Note that one can't, on the basis of such assumptions, argue about the specific sensitivity of Sc systems to cloud-top entrainment instability compared e.g. with radiative and surface-flux forcing, which is still poorly known but is, in model simulations, highly dependent on the specific formulation of the PBL (Stevens, 2002).

Nevertheless, some support for our speculation on the prevalence of buoyancy reversal at the inversion in the SEP is given in Figure 13. Panel (a) highlights the tendency for the vertical gradient of θ_w across the inversion to be negative in periods preceding an increase in h_{inv}, especially in October. These anomalies are then advected northwards. The correlation between the entrainment mass flux (1) and the gradient in θ_w for the area upstream of VOCALS-REx have weak, but marginally significant values for positive lags.

Furthermore, the decomposition used in Figure 12, diagnosed upstream of the VOCALS area between 27S and 30S, indicates much larger and sometimes dominant contributions from entrainment, generally opposing vertical motion but sometimes reinforcing them. In general, the tendencies due to horizontal advection are smaller than at 20S.

To summarise, the evolution of the inversion height may be explained as a combination of fast adjustments on synoptic time-scales, which are partly diabatic and involve a homogenisation of wet-bulb potential

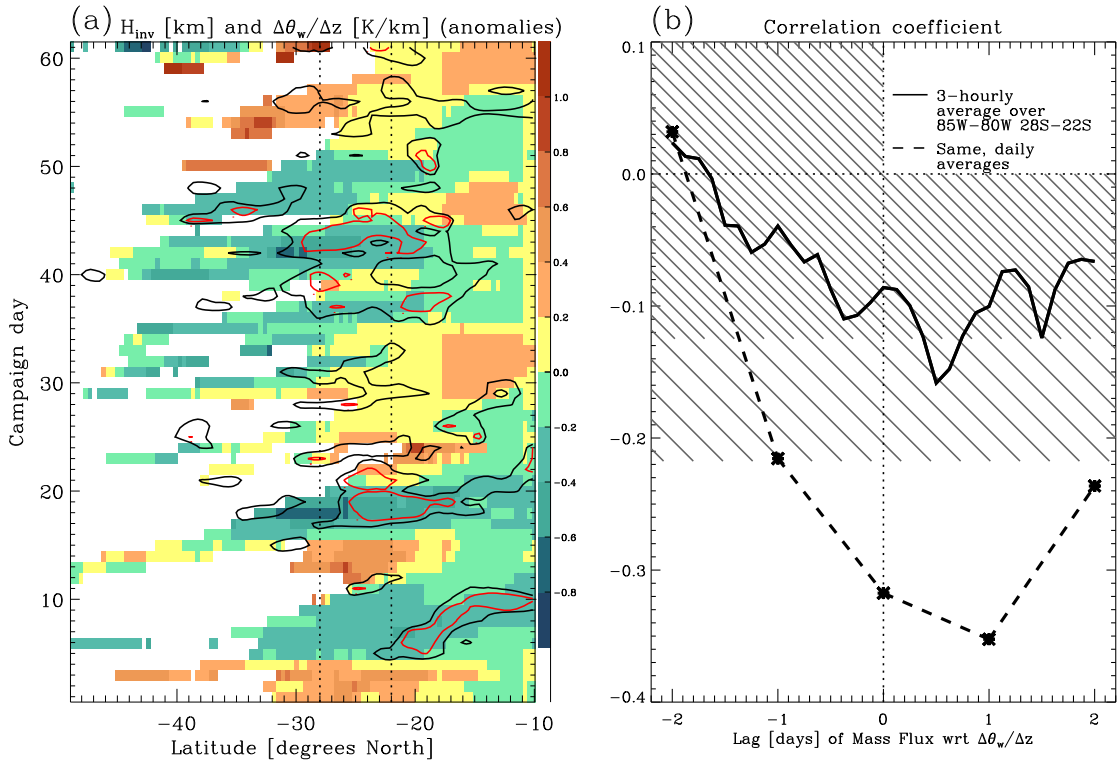

Figure 13: *(a)* Hovmüller diagram (latitude along the abscissae, time along the ordinates) of inversion-height daily-mean anomalies (with respect to the mean over October-November 2008), in colours (scale to the right, in km). Areas where the an inversion (positive temperature gradient) is not diagnosed are left blank. The black contour lines comprise values below -0.5 K/km for the vertical gradient of the wet-bulb potential temperature θ_w; the red lines mark values of -1.5 K/km. All data are averaged between 85W and 80W. *(b)* Lag-correlations of the entrainment mass flux across the inversion and the vertical gradient in wet-bulb potential temperature θ_w. Values within the hatched areas are not formally significant (denser hatching applies to the solid line for 3-hourly data).

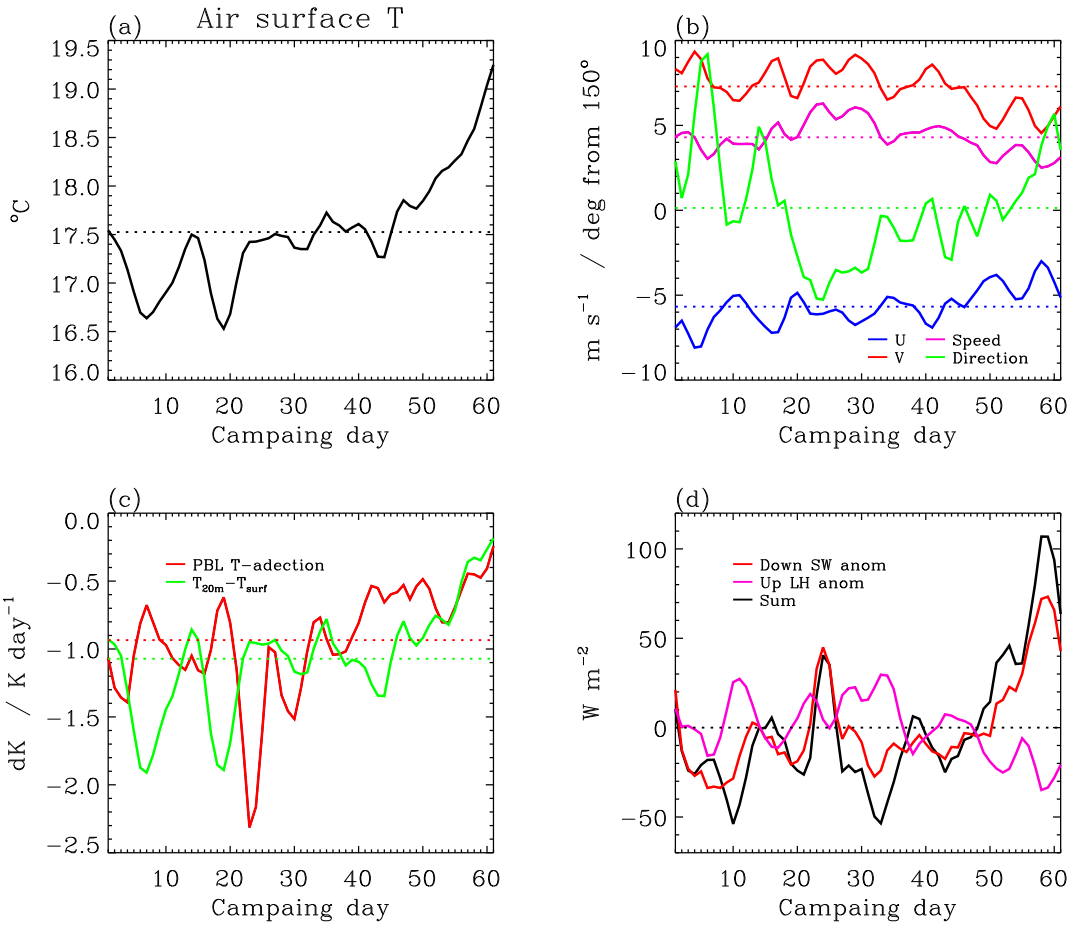

Figure 14: Daily average surface air temperature (a), winds (b), surface air temperature depression and temperature advection (c), and latent and short-wave surface fluxes (d), diagnosed from the UKMO global operational model for the area 90W-80W,25S-15S in October-November 2008.

temperature across the inversion, and a slower evolution driven by changes in the mean subsidence. The latter is mostly driven by the upper-level circulation, with a strong correspondence between poleward flow and anomalous ascent, as required from potential vorticity conservation.

In addition, in the second half of November the MBL was also affected by a comparatively slow but significant warming of the SSTs. The evolution of meteorological parameters at the surface, within the region 90W-80W, 25S-15S, is shown in Figure 14. The air surface temperature undergoes large oscillations in October, becomes fairly stationary between the end of October and the beginning of November, and rises

markedly in the second half of November (panel (a)). The slow evolution largely tracks the SSTs, while the faster oscillations track the changes in atmospheric temperature advection (panel (c)). In the last period, cold advection is reduced, along with the meridional wind (panel (b)), and the temperature of the air raises to approach that of the underlying ocean. This tends to suppress latent heat cooling (panel (d)), which together with the increase in solar irradiation likely contributed to the raise in SSTs. Thus, in late November 2008, the large-scale forcing, with weaker surface wind and large-scale subsidence, combined with the response of regional surface meteorology, to lead a reduction of the stability of the MBL and favour conditions for day-time cloud break-up.

6 Temporal evolution of the large-scale circulation

The change in character of the flow and its variability from the end of October onwards, and the evidence from the composites of Figure 11, suggest a possible link between tropical MBL variability and the location and activity of the mid-latitude storm track.

The storm-track is markedly different between the three distinct periods (discussed in Section 4.2) of VOCALS-REx (Figure 15). In October, upstream of the south-American coast the storm track has a broader meridional spread, with activity at sub-tropical latitudes north of 30^o. A strong interaction with the continental topography is suggested by the maxima on the two sides of it. In early November, by contrast, storms develop in a narrow, sub-polar zonal band, with little evidence of affecting the tropical inversion in

the way indicated in Figure 11. Later still, while baroclinic activity returns north, it appears weak near the South-American coast. This period in the second half of November is also characterised by steady north-westerly mid-tropospheric flow, accompanied by reduced subsidence (Figure 12c).

Although the statistics of the two months under examination is not sufficient to draw firm conclusions, it is interesting to note that the periods with reduced synoptic-scale variability in early November also tends to show lower inversion heights and increased cloud cover. This may be interpreted in terms of the effect that the secondary, ascending circulation associated with the equatorward flank of a storm track can have on the Sc inversion.

The changes in the storm track during the two months of the campaign within the SEP sector reflect,

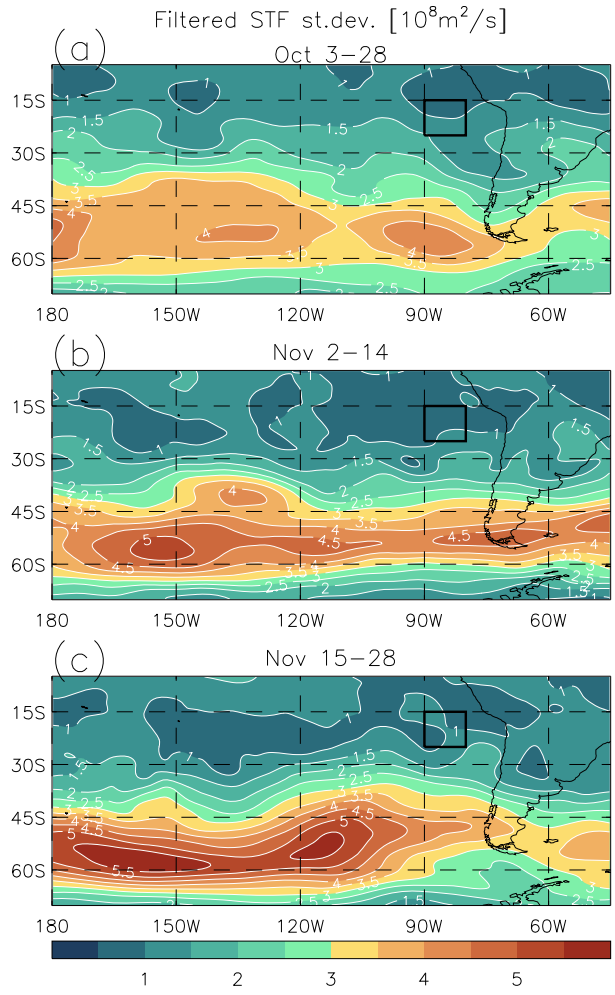

Figure 15: *(a)*, *(b)*, and *(c)*: 6-day running standard deviation of the 1-to-6-day high-pass filtered 50hm streamfunction for three meteorologically distinct periods during the VOCALS-REx campaign. Data from the UKMO operational analyses.

at least in part, the normal seasonal evolution of the large-scale circulation. In general, the spring season is characterised by a large shift in the mid-latitude jet. In the south Pacific, the sub-tropical branch weakens considerably, and a characteristic split-jet structure emerges.

This evolution is represented in Figure 16 for October-November 2008. The subtropical jet, which was prominent during the first half of October, started splitting in favour of a sub-polar component in the second half of the month, and was largely reduced to the Indo-Australian sector in November. Such evolution may

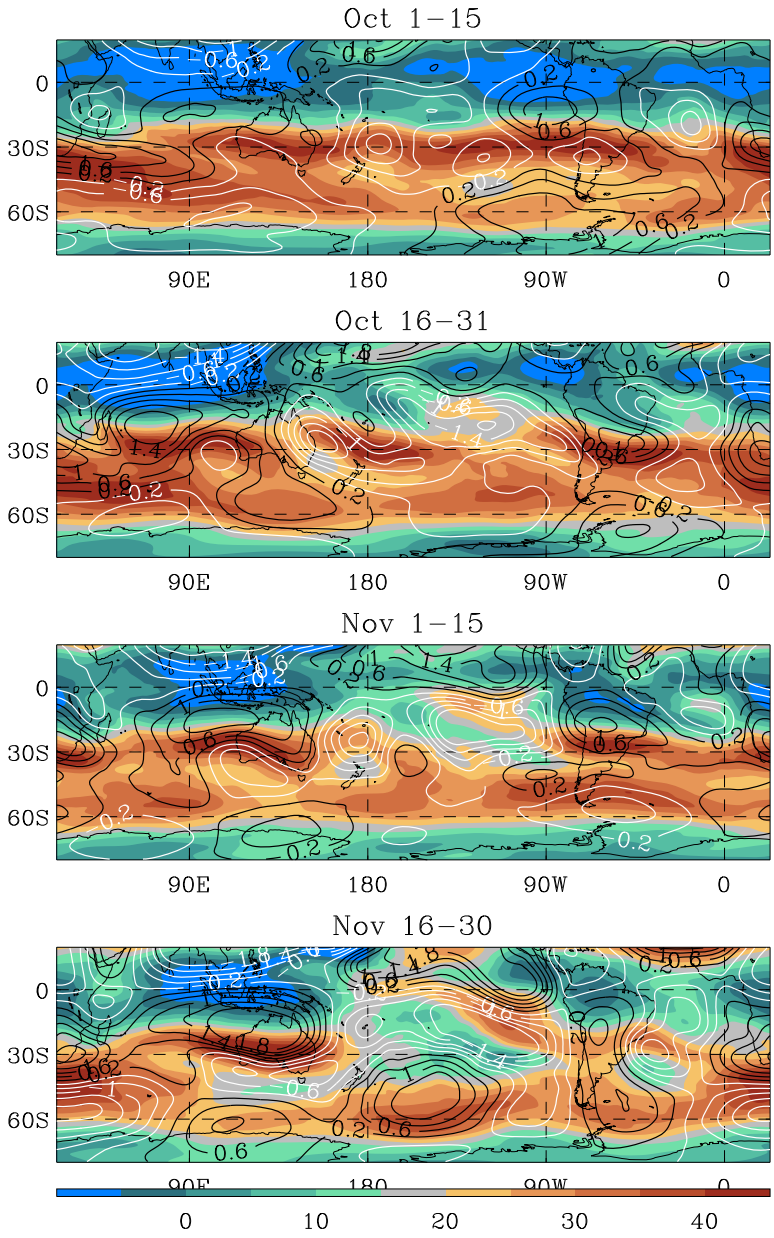

Figure 16: Zonal wind at 200hPa, in units of m/s, for four fortnight periods in October and November 2008 (colour coding, scale at the bottom). Contour lines show the zonally asymmetric component of the 200 hPa streamfunction. Contour interval is $4 \times 10^6 \mathrm{m}^2/\mathrm{s}$; white contours indicate negative values (clockwise, or cyclonic, circulation in the southern hemisphere), and black positive values (anticlockwise, or anticyclonic, circulation). Data from UKMO operational analyses.

explain some of the changes observed in baroclinic activity investing the VOCALS-REx region. Additionally, the subtropical jet initially acts as a wave-guide for any disturbances generated upstream, resulting in very weak persistent wave-like anomaly patterns, hardly escaping tropical latitudes. Starting from the beginning of November, with the break-down of the subtropical jet, and the increased prevalence of (weak) westerlies near the tropical areas of deep convection, a slowly evolving Rossby wave pattern begins to appear, which is well established in the last period of the campaign, with increased cyclonic circulation over the SEP, coincident with northerly flow, dynamically induced lofting, and day-time cloud break-up which characterises the latter part of the campaign.

7 Anomalies and teleconnections

For the duration of the campaign, large-scale SSTs anomalies in the sub-equatorial Pacific indicate a prevalence of weak La-Niña like conditions (Figure 17). In the eastern Pacific, however, SSTs were close to their climatological values. Anomalies in the SEP, as estimated from in-situ and satellite SST products, were less than 0.5 ^{o}C in magnitude, comparable to the discrepancies among such products, and therefore not significant. Among the data-sets used in Figure 17, the NOAA OI most closely matches the in-situ data collected by the R.H.Brown near 20S in November. The UKMO OSTIA product compares even better, but it covers an insufficient temporal span for an estimate of the interannual anomaly. Averages for the single months of October and November do not show additional significant features, although the weak warm anomalies in the Atlantic might have reinforced the relatively subdued convective activity over the Amazon basin.

Consistently with cool central-Pacific conditions, and the corresponding expansion of the Hadley cell, the angular momentum of the atmosphere was reduced compared to its climatological values (not shown). This was accompanied by an increased atmospheric sub-polar meridional temperature gradient, reinforcing the sub-polar jets, especially in October (Figure 18). The large-scale evolution described in the previous section might therefore not be untypical for this season in the southern hemisphere. However, due to these sea-level pressure anomalies, the weakening of the subtropical surface high in the SEP was stronger than usual. Conversely, at the sub-tropical latitudes of VOCALS-REx (north of 45S), synoptic variability, as estimated from the 7-day high-pass filtered variance of the 500hPa streamfunction in the ERA-Interim reanalysis, was below the climatological average for the period 1989-2008, especially in October (not shown). The anomaly

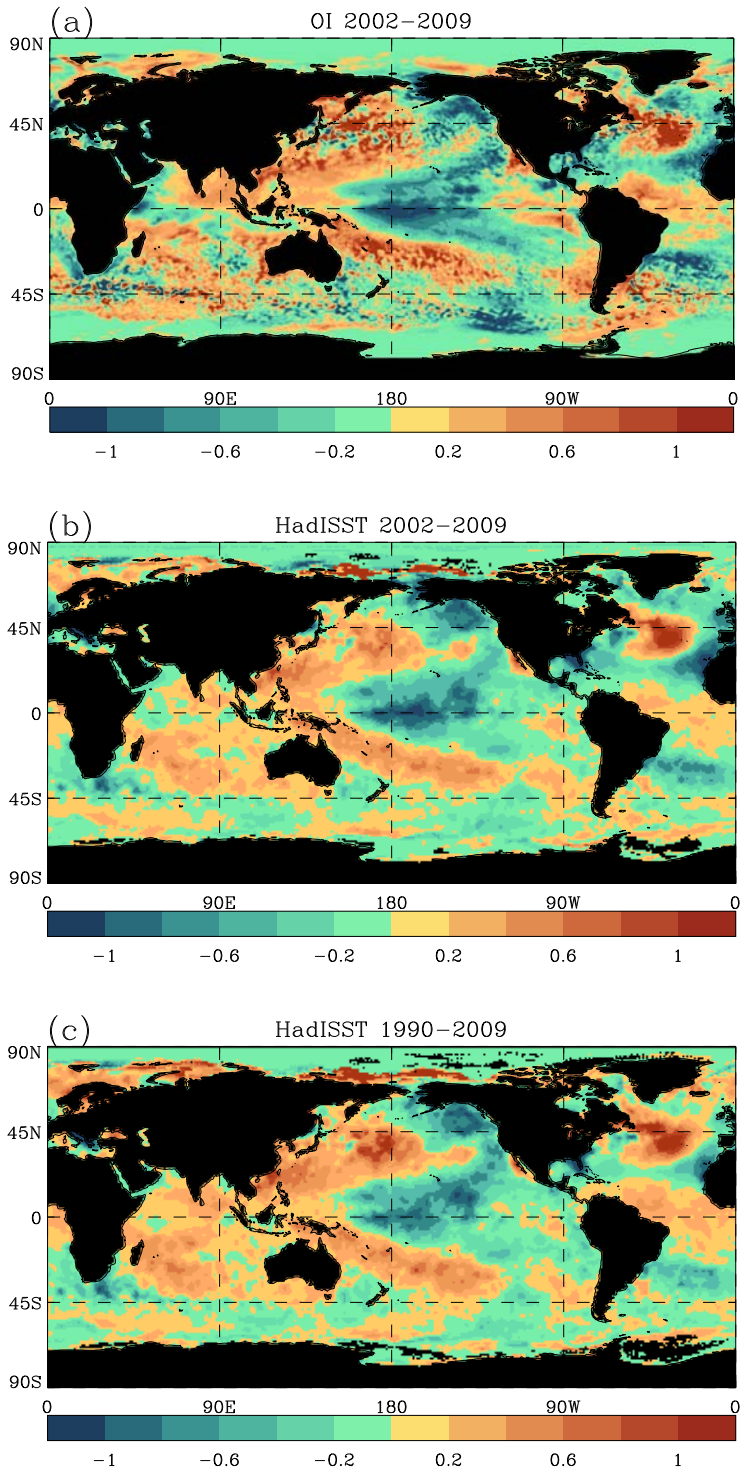

Figure 17: SST anomalies as diagnosed for the period October-November 2008 as estimated from an in-situ (HadISST) and a satellite-derived (NOAA OI v2) product. The reference periods used for the climatologies are given in the title of each panel.

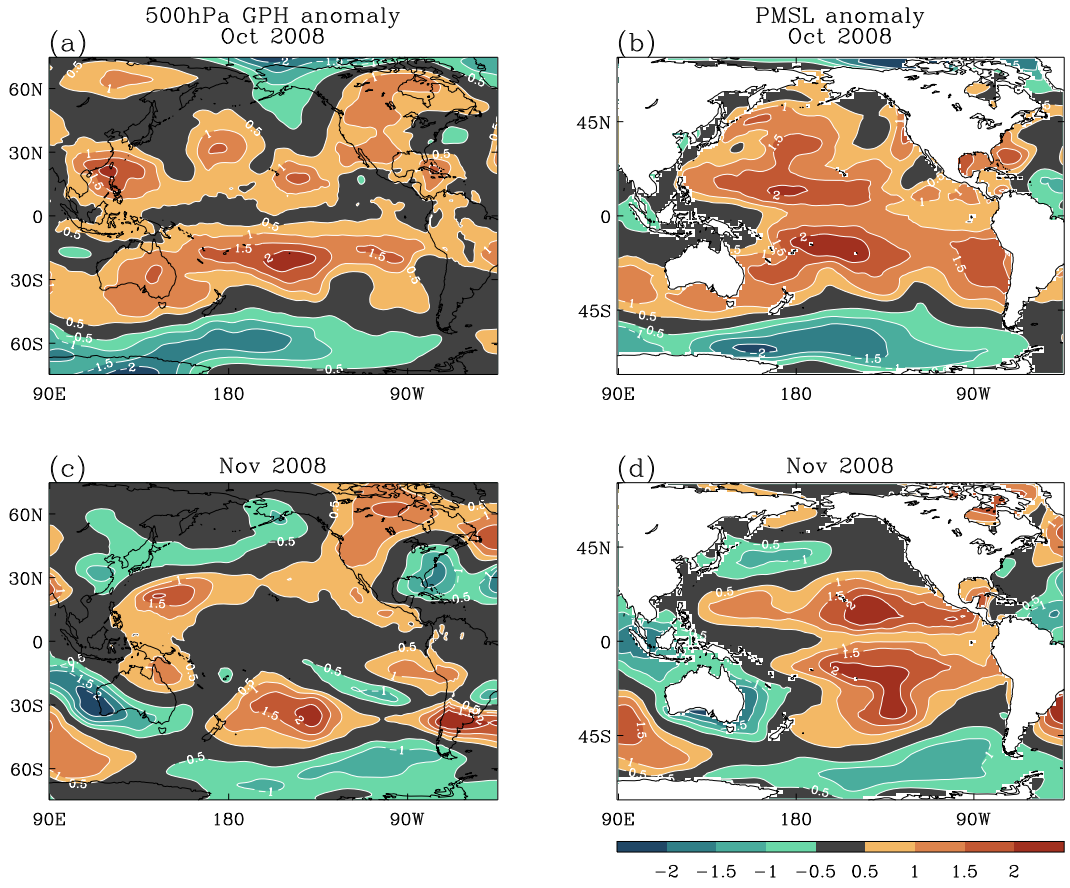

Figure 18: Interannual anomalies for the months of October and November 2008. Panels (a) and (c) show the geopotential height at 500 hPa, panels (b) and (d) the anomalies in sea-level pressure. Reference climatology is for the period 1989-2008. Data from the ERA-Interim reanalysis (Simmons et al., 2006).

resembles that of early November compared to October 2008 (Figure 15, panels (b) and (a), respectively). The implication is that the strong baroclinic activity observed in October to invest the VOCALS-REx area was not by any means exceptional, and the transition to reduced mid-tropospheric synoptic variability probably less marked than normal.

At the end of the previous section we noted that the upper-level circulation in this period appears to have been forced remotely. Consideration of the interannual anomalies confirms and refines these suggestions. Figure 19 shows the interannual anomalies, for the same four periods of Figure 16, of TOA OLR (green contour lines), velocity potential (colour coding), and eddy streamfunction (white contour lines). The Figure

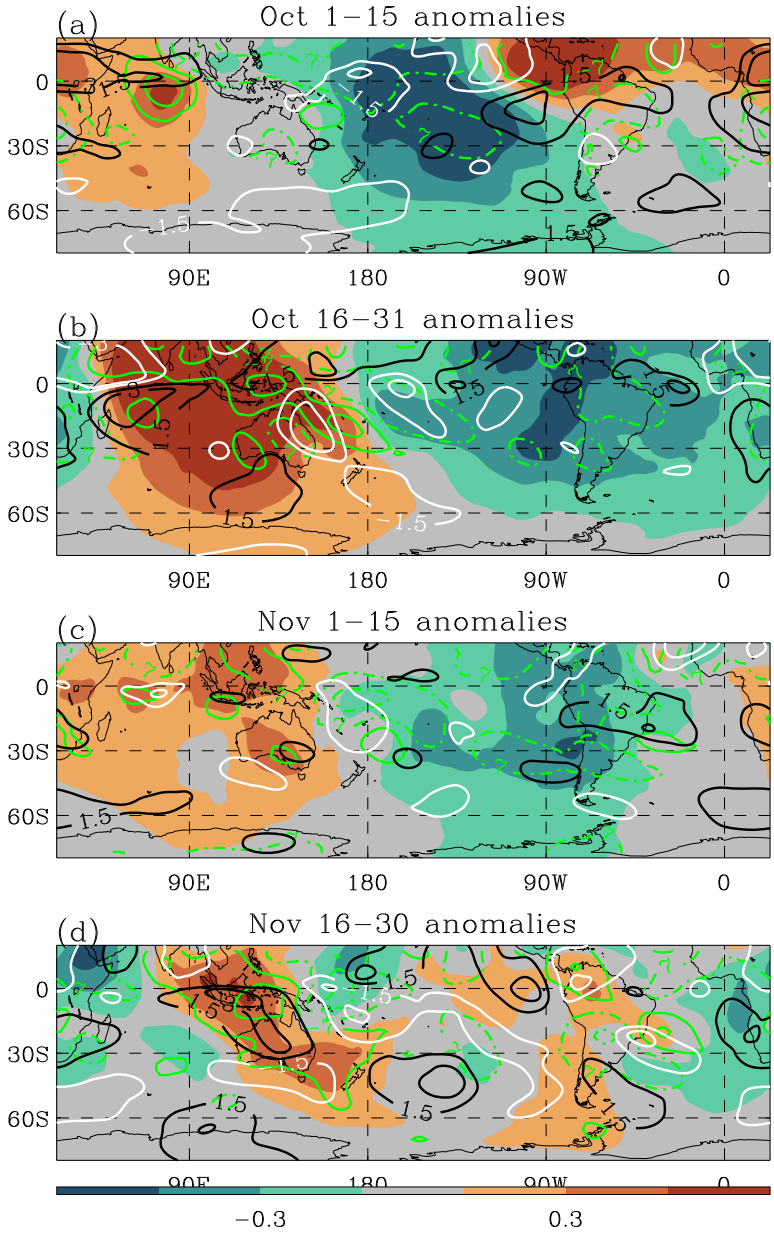

Figure 19: Velocity potential and streamfunction anomalies at 200hPa (colour-coding and black and white contours, respectively) from ERA-Interim, and OLR anomalies (green contours) from the NCEP CDC interpolated OLR data-set, for the four periods of Figure 16. The units for the velocity potential are 10^7 m^2/s, and the contour interval is 2×10^6 m^2/s. The streamfunction anomalies are given in units of the local standard deviation from the 20-year monthly-mean climatology. The contour interval is 1.5, with the zero-line omitted, and contours are black for positive, and white for negative values. For OLR, the contour interval is 7 W/m^2, and contour lines are broken for positive values, and solid for negative values.

highlights the evolution of a positive phase in the MJO, moving from the eastern Indian ocean to the west Pacific between late October and early November. The concomitant velocity-potential and streamfunction anomalies are consistent with a quasi-stationary Rossby wave-train emanating from the region of enhanced convection west of the date-line, which generate a Pacific-South-American (PSA) pattern, with a cyclonic centre in the SEP, in late November. A connection of this type between convective activity in the West Pacific and the occurrence of a PSA pattern of the sign given in Figure 19 has been shown in the climatological context by Mo and Higgins (1998).

8 Diurnal variability

Diurnal variations are an important aspect of the meteorology of the tropical south-east Pacific and the Sc deck. In general, changes in thermal stratification are more significant than the slight variations of the circulation over the MBL, owing to the absence of local moist convection. With increased day-time insolation, the cloud-top warm and the inversion sinks, with concomitant reduction in LWP and reduced cloud cover. This process is extremely important in terms of insolation at the sea surface, as the diurnal cloud-cover minimum occurs a few hours after the maximum in solar irradiation, so that accurate representation of the diurnal cloud evolution appears crucial.

The UKMO forecast model relies on MBL turbulence parametrisations to represent the processes that drive the diurnal cycle in the MBL. The simulated a diurnal cycle in fractional cloud-cover and PBL depth is in good qualitative agreement with observations, as long as only maritime areas well away from the coast are considered (Abel et al. 2010). The simulated mean diurnal variations have the same qualitative character as an adiabatic night-time lifting and day-time sinking of the cloud top, concomitant with a reduction or increase, respectively, of the lower-tropospheric temperature, and an increase and reduction, respectively, of the cloud liquid water concentration (Figure 20). This may be contrasted with the variability on synoptic time-scales, which we have seen to lead to a correlation between changes in cloud cover and in the inversion height of the opposite sign.

Superimposed on this locally, radiatively driven diurnal cycle, a number of authors (Garreaud and Munoz 2004; Wood et al. 2009; Rahn and Garreaud 2010a) have studied the diurnal modulation of the vertical wind in the SEP by regular gravity-wave pulses propagating offshore from the South-American coast. Such

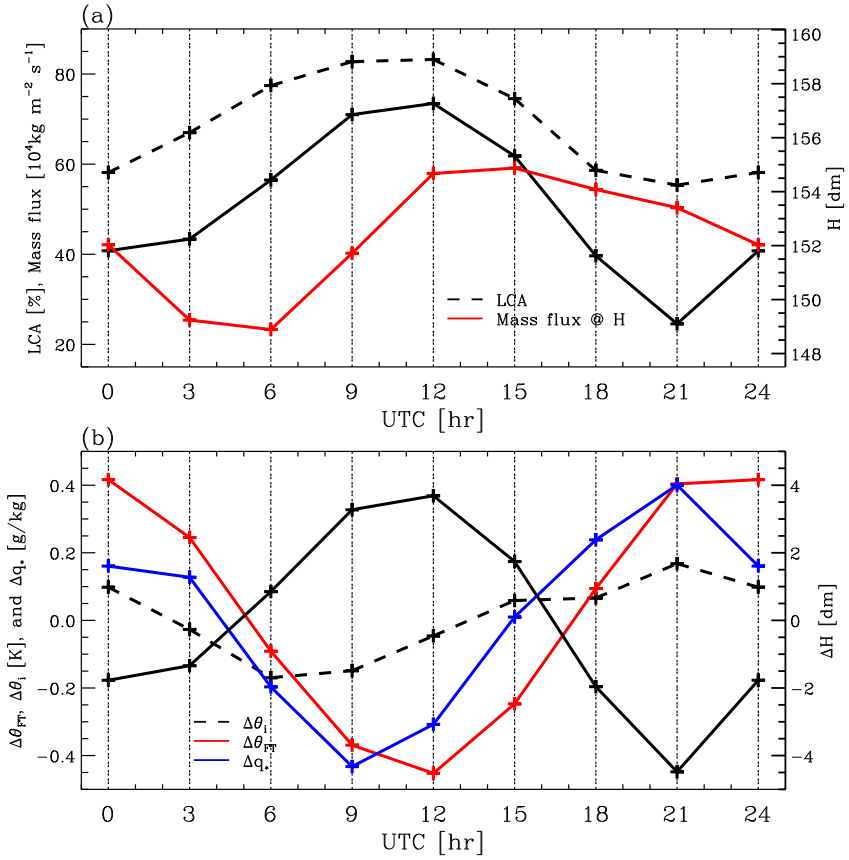

Figure 20: Mean diurnal evolution of thermodynamic quantities near the inversion in the area 15S-25S, 90W-80W. (a) Inversion height (solid black line), cloud amount (broken line), and diagnosed mass entrainment across the inversion (red line) as a function of time of the day. (b) Inversion height anomalies (solid line) together with the lower-tropospheric (z =2200m) potential temperature (red line), the MBL-top potential temperature (broken line), and the MBL-top saturation mixing ratio (blue line) as a function of the time of the day. Data from the UKMO operational analyses and 3h-21h forecasts.

pulses affect the entire depth of the troposphere. They are associated with diurnal heating over the Andean mountain ranges, and they have a measurable effect on lower-tropospheric temperatures and the MBL-depth (Garreaud and Munoz, 2004), and on cloud liquid water (Wood et al., 2002). Figure 21 shows the associated, daily circulation anomalies for a transect along a great circle that intersects the Peruvian Andes. The mid-

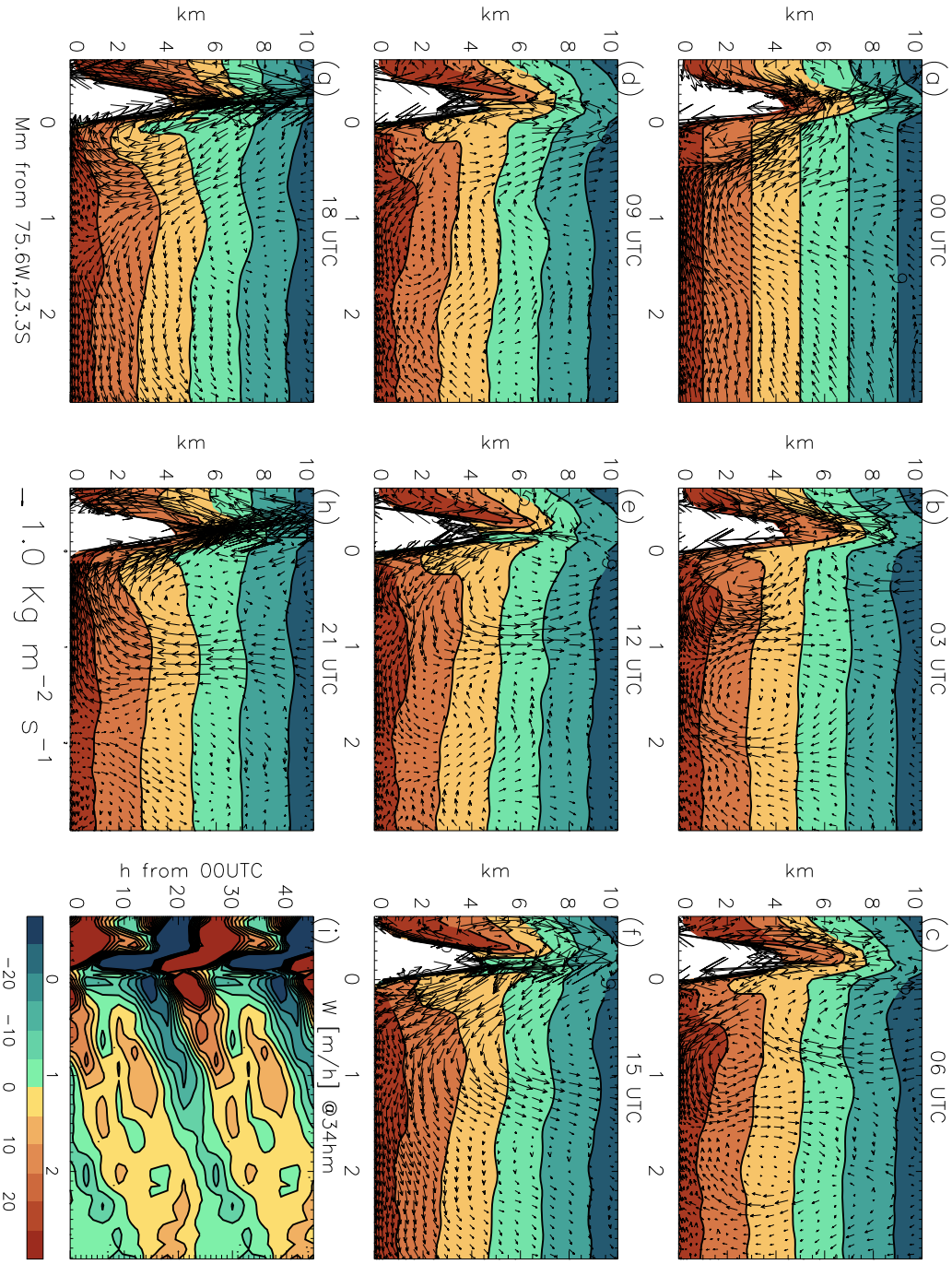

Figure 21: *(a)-(h)*: Snapshots of the mean circulation through a daily cycle along a great-circle at a right angle to the South-Peruvian orographic slope and intersecting the coastline at 75.6W, 23.3S. The long-term mean circulation has been removed and average anomalies for the time of the day are shown as indicated at the top of each panel in hours UTC. The abscissae indicate offshore distances in Mm, and the ordinates vertical heights in km. The arrows represent two components of the flow, the offshore and the vertical mass fluxes (scale arrow at the bottom of panel (h)). The colour-filled contour lines depict the nominal displacement of constant-height surfaces at 00z (panel (a), shown at intervals of 2km starting from 1km) as obtained from the time-integrated

afternoon mountain breeze maximum (21z) excites a second-baroclinic-mode gravity-wave circulation (0z) that propagates offshore. In the lower troposphere, below the top of the mountain ridge (5km), a positive vertical wind anomaly moves in the south-south-west direction with a speed of approximately 25 m/s (see upward arrows near 20S at 0z, and near 26S at 9z in the Figure). Maps of vertical wind anomalies highlighting this ascending wave are shown in Garreaud and Munoz (2004) and Wood et al. (2009) using different data sources, model simulations and periods of time, demonstrating that its regular occurrence is robust and well-captured in model simulation, although there can be errors in the exact timing (Rahn and Garreaud, 2010a). Somewhat weaker gravity waves also emanate and propagate zonally from the meridionally oriented ridge of the Chilean Andes (Garreaud and Munoz 2004).

That a combination of different waves with different origins, phases and time-scales is at play is suggested by the maps of Figure 22, which shows the phases of the Fourier components of the vertical velocity at 5800m with periods of 24 hours and 12 hours, as well as the times of maximum and minimum, for the mean diurnal cycle at each location. The phase lines of the 24-hour component are broadly parallel to the Peruvian cordillera, suggesting propagation away from it. They indicate a horizontal scale of roughly 3000km, and tend to correspond to the time of maximum subsidence (+12h). The 12-hour component appears to involve smaller spatial scales and also smaller phase speeds. While its phase lines are also mainly aligned with the Peruvian coastline, a distinct, meridionally oriented area appears off the Chilean coast, indicating zonal offshore progression. Near the land-mass, its timing is close to the timing of the maximum vertical wind, i.e. anomalous ascending motion. This is consistent with the short duration of the ascending wave discussed by Garreaud and Munoz (2004) which appears to mainly depend on dry the mountain-breeze systems on the western and south-western sloped of the Andes. In addition, Munoz (2008) demonstrated that within about 10^o west of the Chilean coast, differential subsidence associated with increased heating of the Andean slopes in the North has a leading-order effect on the diurnal variations of the MBL-depth and the surface pressure gradient, affecting the low-level jet and driving diurnal variations of the surface winds. These processes are likely to exert a significant control on the diurnal cycle in the area most intensively observed during VOCALS-REx (Zuidema et al., 2010). More generally, they indicate that the interplay between local, meso-scale, and large-scale processes can be very important.

The diurnal cycle over the SEP thus is forced by a combination of local irradiation, and gravity waves

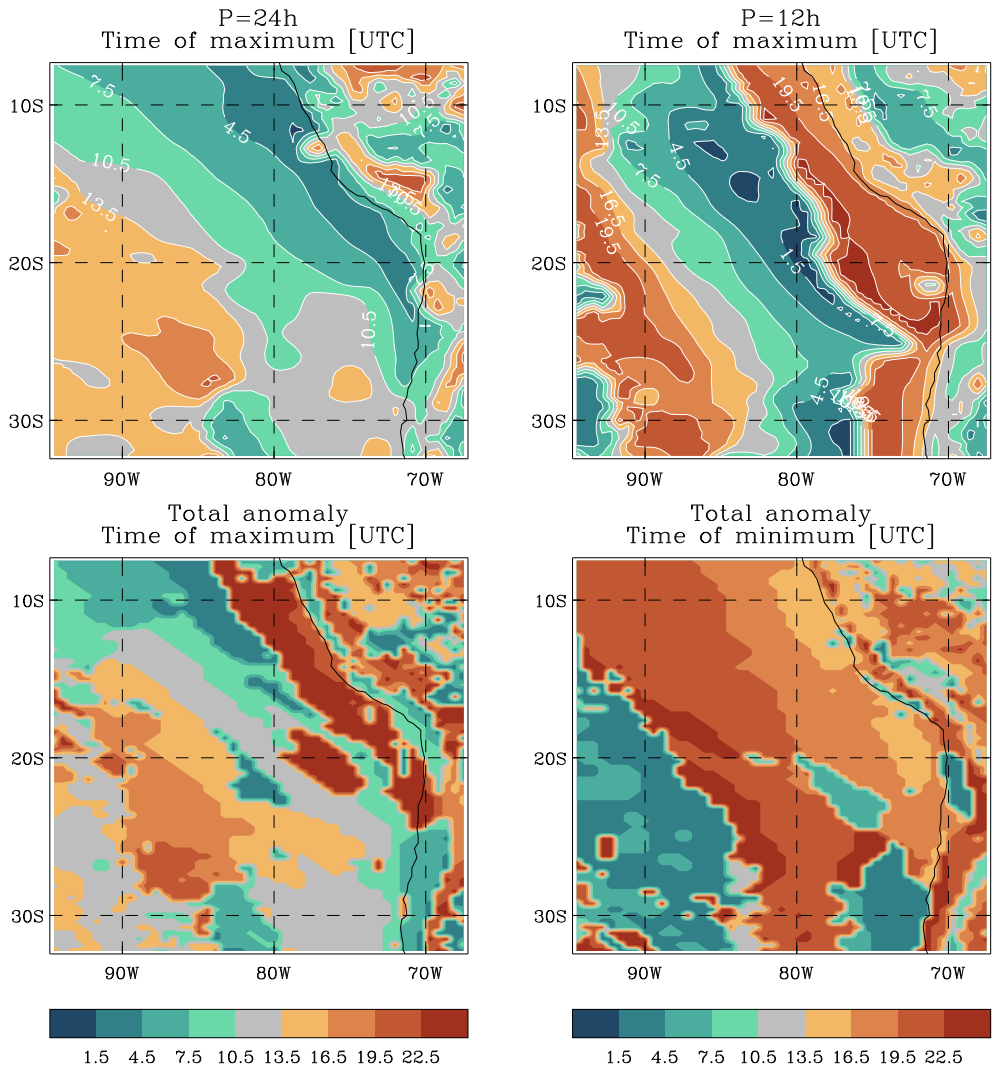

Figure 22: Top: negative phase offset, in hours, of the cosine component of 24-hour (left) and 12-hour (right) period of the vertical velocity anomalies at 5800m for the mean diurnal cycle in the SEP. Bottom: approximate time of maximum (positive, left) and time of minimum (negative, right) in the 5800m vertical wind anomalies. The data frequency used, from the UKMO model, is three-hourly (operational analyses plus 3h-21h forecasts).

emanating from the predominantly dry regional mountain breeze systems. Differential heating of the slopes with different exposure to solar irradiation is undoubtedly a significant factor in determining the overall pattern and timing of the diurnal cycle in the SEP (Munoz 2008). To what extent continental moist

convective activity further afield on the eastern and northern side of the orography, and interactions with the vigorous time-mean zonal flow that crosses the orographic barrier, affect this pattern is still an open question. Isolating the sources of forcing of the diurnal cycle in the SEP, and disentangling their effect, is the objective of current investigation.

9 Summary and conclusions

We have presented an overview of the meteorological conditions in the Sc-covered area of the subtropical anticyclone in the south-east Pacific during the period October-November 2008 when the VOCALS-REx intensive observations campaign took place. The region of interest spans an area around the 20S parallel between the coast and 90W. As VOCALS-REx was focussed on conditions in the maritime boundary layer (MBL), with its capping inversion and its extensive Sc cloud deck, we chiefly analyse conditions in the lower troposphere and how they varied in dependence of the circulation.

We have shown a link between the amount of low cloud present and the depth of the MBL, diagnosed as the height where the capping inversion is located. The link is consistent with the known relation between low-cloud liquid water and the "lower-tropospheric stability" (LTS) diagnostics (Klein and Hartmann, 1993; George and Wood, 2010), as well as with the relationship between the circulation and anomalies in Sc cover over subseasonal time-scales (Xu et al. 2005). Consistently with these studies, which indicate a prevalent atmospheric control on the subseasonal variability of the Sc desk, we suggest that the emergence of this link depends on the stability of the stratification across the inversion and corresponds to the maintenance of a near-vanishing jump in wet-bulb potential temperature, facilitating cloud-top entrainment.

During the period of the study, changes in the inversion height, and the associated cloud cover, occurred over several time-scales. In the area of interest, they were initially (until late October) predominantly associated with the horizontal advection of inversion-height anomalies generated upstream until late October.

Later, changes in the vertical velocity were most important. We confirm the results of Rahn and Garreaud (2010b). Diabatic effects however are not negligible, and they contribute especially with the changes in cloud cover on short time-scales, from one day to the next. This might be expected from the nature of the mean flow across the inversion, which requires entrainment in order to be maintained, and involves the horizontal as well as the vertical winds.

The most striking influence on the subtropical latitudes that were sampled comes from baroclinic systems originating in the southern-hemisphere storm track and located or moving north far enough to interact with the Andean orography. As the ridge is oriented in a north-south direction, and spans the depth of the lower half of the cyclones, storms are delayed in its vicinity, gradually weakening on the western side and re-forming on the eastern side of the mountain chain (Vera et al., 2002). During this time, significant temperature advection occurs in the mid-troposphere (mostly vertical and meridional), which is associated with large changes in the height of the inversion and strongly affects the cloud fields. Near the coast, along-slope flows associated with the pressure anomalies of the synoptic systems (Xu et al., 2005; Garreaud and Rutllant, 2003) contribute to alter the stratification in the lower troposphere and thus further affect the cloud. The interaction between sub-tropical cyclones and the Andean orography appears thus to play a significant role for the variability of the Sc deck, and, by implication, on the climate of the SEP.

Additionally, between the end of October and the first half of November a mid-tropospheric anticyclonic anomaly developped to the North of 20S, following periods of intense precipitation over northern South America. The anticyclone moved upstream (westwards), increasing the meridional temperature gradient until cyclone waves appeared at its southern flank, upstream of the VOCALS-REx area. More significantly, however, it caused the advection of air-masses lofted by convection over the continent into the middle and lower troposphere above the SEP, potentially giving a significant contribution to aerosol load there. Given that October and November 2008 overall saw reduced precipitation over South America compared with the climatology, it is possible that events like this are normally more common than was observed during the campaign. A similar effect on air-mass origin in the SEP resulted from an intense cyclone that occurred between 21-23 October, in association with the strong mid-tropospheric ridging (of smaller spatial scale and shorter duration than the November case) that preceded it.

The slower evolution of the MBL inversion and its cloud depends on changes in the large-scale circulation, especially to the extent in which they affect tropospheric subsidence. A southward shift in the overall position of the storm track between late October and early November, which is part of the normal seasonal evolution, and, in late November, a quasi-stationary planetary wave patter, with a low centred over the SEP, and likely to have originated from convective activity anomalies in the west Pacific associated with the passage of an MJO event, are identified as factor affecting the VOCALS-REx campaign.

We also discussed the presence and possible significance of interannual anomalies during VOCALS-REx. Large-scale SSTs had a La-Nina-like anomaly pattern, and, consistently, the jet-streams were displaced further poleward than usual. At the same time, surface pressure was higher than usual in the sub-tropical anticyclone, to weaken to near-climatology later. Thus, the effect of mid-latitude storms on the SEP might have been weaker than usual during the VOCALS-REx period, while the slower seasonal changes were amplified. The concurrent anomalies in tropical precipitation (subdued over South America, and an active MJO phase occurred in the Indo-Pacific sector) and the circulation anomalies in the SEP reflected known patterns of subseasonal variability (Mo and Higgins, 1998; Robertson and Mechoso, 2000).

Finally, we give a brief overview of the mean diurnal cycle in MBL depth over the SEP (), which results from a combination of local, radiatively driven changes in the MBL structure, and remotely forced vertical velocity anomalies that propagate into the SEP from the Peruvian and Chilean cordilleras as internal gravity waves.

Acknowledgements NOAA OI SST V2 data provided by the NOAA/OAR/ESRL PSD, Boulder, Colorado, USA, from their Web site at http://www.esrl.noaa.gov/psd/. TT is grateful, for discussions and suggestions, to Steve Woolnough and to other members of the Tropical Group at the Department of Meteorology of the University of Reading.

References

Abel, S.J., D.N. Walters, and G. Allen, 2010: Evaluation of stratocumulus cloud prediction in the Met Office forecast model during VOCALS-REx. Atmos. Chem. Phys. 2010

Barret, B.S., R.D. Garreaud, and M. Falvey, 2009: Effect of the Andes cordillera on precipitation from a midlatitude cold front. Mon. Weather Rev. 137, 3092-3109.

Berner, A. and Bretherton, C. S., 2010: Large-eddy simulation of the VOCALS RF06 pocket of open cells: cloud macrostructure, entrainment and maintenance timescale of microphysical gradients. Manuscript in preparation.

Bretherton, C. S., Uttal, T., Fairall, C. W., Yuter, S. E., Weller, R. A., Baumgardner, D., Comstock, K., and Wood, R.: The EPIC 2001 stratocumulus study, B. Am. Meteor. Soc., 85, 967 977, 2004.

Bretherton, C.S., R. Wood, R.C. George, D. Leon, G. Allen, and X. Zheng, 2010: Southeast Pacific strtocumulus clouds, precipitation and boundary layer structure sampled along 20S during VOCALS-REx. Atmos. Chem. Phys. 2010

Bony, S., and Dufresne, J.-L., 2005: Marine boundary layer clouds at the heart of tropical cloud feedback uncertainties in climate models. Geophys.Res.Lett. 32, L20806

Colbo, K., and R.A. Weller, 2007: The variability and heat budget of the upper ocean under the Chile-Peru stratus. J.Mar.Res. 65:607 637.

de Szoeke, S.P., and S.-P. Xie, 2008: The tropical eastern Pacific seasonal cycle: assessment of errors and mechanisms in IPCC AR4 coupled ocean-atmosphere general circulation models. J.Clim. 21, 2573-2590

Deardorff, J.W., 1980: Cloud top entrainment instability. J.Atmos.Sci. 37, 131-147.

Garreaud, R.D., J. Rutllant, and H. Fuenzalida, 2002: Coastal lows along the subtropical west coast of south America: mean structure and evolution. Mon. Weather Rev. 130, 75-88

Garreaud, R.D., and J. Rutllant, 2003: Coastal lows along the subtropical west coast of south America: numerical simulation of a typical case. Mon. Weather Rev. 131, 891-908

Garread, R.D., and R. Muñoz, 2004: The diurnal cycle in circulation and cloudiness over the subtropical southeast Pacific: a modelling study. J. Clim. 17, 1699-1710.

George, R.C., and R. Wood, 2010: Subseasonal variability of low cloud radiative properties over the southeast Pacific ocean. Atmos. Chem. Phys. 10, 4047-4063

Hastenrath, S., 1991: Climate Dynamics of the Tropics, Kluwer, Dordrecht, 1991

Klein, S.A., and D.L. Hartmann, 1993: The seasonal cycle of low stratiform clouds. J.Clim. 6, 1587-1606.

Konor, C.S., G.C. Boezio, C.R. Mechoso, and A. Arakawa, 2009: Parameterization of PBL processes in an atmopsheric general circulation model: descriptiona dn preliminary assessment. Mon.Weather Rev. 137, 1061-1082

Ma, C.-C., C.R. Mechoso, A.W. Robertson, and A. Arakawa, 1996: Peruvian stratus cloud and the tropical Pacific circulation: a coupled ocean-atmosphere study. J. Clim. 9, 1635-1645

Mo, K.C., and R.W. Higgins (1998) The Pacific-South American Modes and Tropical Convection during the Southern Hemisphere Winter. Mon. Wea. Rev., 126: 1581-1596.

Munoz, R.C., and R.D. Garreaud, 2005: Dynamics of the low-level jet off the west coast of subtropical

south America. Mon. Weather Rev. 133, 3661-3677.

Munoz, R.C., 2008: Diurnal cycle of surface winds over the subtropical southeast Pacific. J. Geophys. Res. 113, D13107 (doi:10.1029/2008JD009957)

Rahn, D.A., and R. Garreaud, 2010a: Marine boundary layer over the subtropical southeast Pacific during VOCALS-REx - part 1: mean structure and diurnal cycle. Atmos. CHem. Phys. 10, 4491-4506.

Rahn, D.A., and R. Garreaud, 2010b: Marine boundary layer over the subtropical southeast Pacific during VOCALS-REx - part 2: synoptic variability. Atmos. CHem. Phys. 10, 4507-4519.

Reynolds, R.W., N.A. Rayner, T.M. Smith, D.C. Stokes, and W. Wang, 2002: An improved in situ and satellite SST analysis for climate. J. Climate, 15, 1609-1625.

Richter, I., and C.R. Mechoso, 2006: Orographic influences on subtropical stratocumulus. J. Atmos. Sci. 63, 2585-2601

Robertson, A. W. and C. R. Mechoso (2000) Interannual and interdecadal variability of the South Atlantic Convergence Zone. Mon. Wea. Rev.,128: 2947-2957.

Rozendaal, M. A., C. B. Leovy, and S. A. Klein, 1995: An observational study of diurnal variations of the marine stratiform clouds. J. Climate, 8, 1795-1809.

Painemal, D., R.D. Garreaud, J. Rutllant, and P. Zuidema, 2010: Southeast Pacific stratocumulus: high-frequency variability and mesoscale structures over San Felix island. J.App.Meteor.Clim. 49, 463-477

Seleuchi, M.E., R.D. Garreaud, F.A. Norte, and A.C. Saulo, 2006: Influence of sutropicalAndes on baroclinic disturbances: a cold front case study. Mon. Weather Rev. 14, 3317-3334

Shaffrey, L.C., I. Stevens, W.A. Norton, M.J. Roberts, P.L. Vidale, J.D. Harle, A. Jrrar, D.P. Stevens, M.J. Woodage, M.E. Demory, J. Donners, D.B. Clark, A. Clayton, J.W. Cole, S.S. Wilson, W.M. Connolley, T.M. Davies, A.M. Iwi, T.C. Johns, J.C. King, A.L. New, J.M. Slingo, A. Slingo, L. Steenman-Clark, and G.M. Martin, 2009: UK-HiGEM: The new UK High resolution Global Environment Model. Model description and basic evaluation. Vol. 22, p. 1861-1896.

Shao, H., and G. Liu (2004), Detecting drizzle in marine warm clouds using combined visible, infrared, and microwave satellite data, J. Geophys. Res., 109, D07205, doi:10.1029/2003JD004286.

Simmons, A., S. Uppala, D. Dee, S. Kobayashi, 2006: ERA-Interim: New ECMWF reanalysis products from 1989 onwards. ECMWF Newsletter No.110, 25-35

Stark, J.D., C.J. Donlon, M.J. Martin and M.E. McCulloch, 2007: OSTIA: An operational, high resolution, real time, global sea surface temperature analysis system. Oceans '07 IEEE Aberdeen, conference proceedings. Marine challenges: coastline to deep sea. Aberdeen, Scotland. IEEE.

Stevens, B., 2002: Entrainment in stratocumulus topped mixed layers. Q.J.R.Meteorol. Soc. 119, 2663-2689.

Takahashi, K., and D.S. Battisti, 2006: Processes controlling the mean tropical Pacific precipitation pattern. Part I: the Andes and the easter Pacific ITCZ. J. Clim. 20, 3434-3451.

Vera, C.S., P.K. Vigliarolo, and E.H. Berbery, 2002: Cold season synoptic-scale waves over subtropical south America. Mon. Weather Rev. 130, 684-699.

Wang, H., Feingold, G., Wood, R., and Kazil, J., 2010: Modelling microphysical and meteorological controls on precipitation and cloud cellular structures in Southeast Pacific stratocumulus, Atmos. Chem. Phys., 10, 6347-6362, doi:10.5194/acp-10-6347-2010.

Wood, R., Bretherton, C. S., and Hartmann, D. L.: Diurnal cycle of liquid water path over the subtropical and tropical oceans, Geophys. Res. Lett., 29, 2092, doi:1029/2002GL015371, 2002.

Wood, R., and C.S. Bretherton, 2006: On the relationship between stratiform low cloud cover and lower-tropospheric stability. J. Clim. 19, 6425-6432.

Wood, R., and Hartmann, D.L., 2006: Spatial variability of liquid water path in marine low cloud: the importance of mesoscale cellular convection. J. Clim. 19, 1748-1764

Wood, R., M. Köhler, R. Bennartz, and C. O'Dell, 2009: The diurnal cycle of surface divergence over the global oceans. Q.J.R.Meteorol.Soc. 135, 1484-1493

Wood, R., C.S. Bretherton, C.R. Mechoso, R.A. Weller, B. Huebert, F. Straneo, B.A. Albrecht, H. Coe, G. Allen, G. Vaughan, P. Daum, C. Fairall, D. Chand, L. Gallardo Klenner, R. Garreaud, C. Grados Quispe, D.S. Covert, T. S. Bates, R. Krejci, L.M. Russell, S. de Szoeke, A. Brewer, S.E. Yuter, S.R. Springston, A. Chaigneau, T. Toniazzo, P. Minnis, R. Palikonda, S.J. Abel, W.O.J. Brown, S. Williams, J. Fochesatto, and J. Brioude, 2010: The VAMOS Ocean-Cloud-Atmosphere-Land Study Regional Experiment (VOCALS-REx): goals, platforms, and field operations. Atmos. Chem. Phys., 2010

Wyant, M. C., Wood, R., Bretherton, C. S., Mechoso, C. R., Bacmeister, J., Balmaseda, M. A., Barrett, B., Codron, F., Earnshaw, P., Fast, J., Hannay, C., Kaiser, J. W., Kitagawa, H., Klein, S. A., Köhler, M.,

Manganello, J., Pan, H.-L., Sun, F., Wang, S., and Wang, Y.: The PreVOCA experiment: modeling the lower troposphere in the Southeast Pacific, Atmos. Chem. Phys., 10, 4757 4774, doi:10.5194/acp-10-4757-2010, 2010.

Xu, H., S.-P. Xie, and Y. Wang, 2005: Subseasonal variability of the southeast Pacific stratus cloud deck. J. Clim., 18, 131-142.

Zheng, Y., T. Shinoda, G.N. Kiladis, J. Lin, E.J. Metzger, H.E. Hurlburt, and B.S. Giese, 2010: Upper-ocean processe under the stratus cloud deck in the southeast Pacific ocean, J. Phys. Oceanog. 40, 103-120

Zuidema, P., D. Painemal, S. de Szoeke, and C. Fairall, 2009: Stratocumulus cloud-top height estimated and their climatic implications. J. Clim. 22, 4652-4665